Eichen, Elliot Gene

SPECKLE MEASUREMENTS WITH A CCD ARRAY: APPLICATIONS TO SPECKLE REDUCTION

The University of Arizona PH.D. 1982

PLEASE NOTE:

In all cases this material has been filmed in the best possible way from the available copy. Problems encountered with this document have been identified here with a check mark __√__.

1. Glossy photographs or pages __√__
2. Colored illustrations, paper or print _____
3. Photographs with dark background __√__
4. Illustrations are poor copy _____
5. Pages with black marks, not original copy _____
6. Print shows through as there is text on both sides of page _____
7. Indistinct, broken or small print on several pages _____
8. Print exceeds margin requirements _____
9. Tightly bound copy with print lost in spine _____
10. Computer printout pages with indistinct print _____
11. Page(s) _____ lacking when material received, and not available from school or author.
12. Page(s) _____ seem to be missing in numbering only as text follows.
13. Two pages numbered _____. Text follows.
14. Curling and wrinkled pages _____
15. Other _____

SPECKLE MEASUREMENTS WITH A CCD ARRAY: APPLICATIONS TO SPECKLE REDUCTION

by

Elliot Gene Eichen

A Dissertation Submitted to the Faculty of the

COMMITTEE ON OPTICAL SCIENCES (GRADUATE)

In Partial Fulfillment of the Requirements
For the Degree of

DOCTOR OF PHILOSOPHY

In the Graduate College

THE UNIVERSITY OF ARIZONA

1 9 8 2

THE UNIVERSITY OF ARIZONA
GRADUATE COLLEGE

As members of the Final Examination Committee, we certify that we have read the dissertation prepared by Elliot Gene Eichen

entitled Speckle Measurements with a CCD Array: Applications to Speckle Reduction

and recommend that it be accepted as fulfilling the dissertation requirement for the Degree of Doctor of Philosophy.

James C. Wyant	1/20/82
	Date
[illegible]	1/20/82
	Date
B. Ray Frieden	1/20/82
	Date
	Date
	Date

Final approval and acceptance of this dissertation is contingent upon the candidate's submission of the final copy of the dissertation to the Graduate College.

I hereby certify that I have read this dissertation prepared under my direction and recommend that it be accepted as fulfilling the dissertation requirement.

James C. Wyant — 1/28/82

Dissertation Director — Date

STATEMENT BY AUTHOR

This dissertation has been submitted in partial fulfillment of requirements for an advanced degree at The University of Arizona and is deposited in the University Library to be made available to borrowers under rules of the Library.

Brief quotations from this dissertation are allowable without special permission, provided that accurate acknowledgment of source is made. Requests for permission for extended quotation from or reproduction of this manuscript in whole or in part may be granted by the head of the major department or the Dean of the Graduate College when in his judgment the proposed use of the material is in the interests of scholarship. In all other instances, however, permission must be obtained from the author.

SIGNED: Elliot Jane Eichen

To my parents, my brothers, and my wife

ACKNOWLEDGMENTS

It is a delight to acknowledge the guidance and patience of my dissertation director, Jim Wyant. Professor Wyant's technical advice and time were invaluable for completing this work; his interest in the careers of his students and his encouragement to publish and present papers is exemplary.

Dr. Gudmunn Slettemoen made several suggestions to the early theory developed in Chapter 2, and in general helped with my understanding of speckle phenomena. I am grateful to Kais Al-Marzouk for the Dektak surface profiles found in Chapter 4, to Ted Hadley for his assistance with the electronics, and to David Forbes for his help with the software.

My thanks go to Sherrie Cornett for typing and her advice on style and format, to Kathy Seeley for editing the first three chapters, and to Don Cowen for the illustrations.

For moral encouragement, basketball games, and requiring me to remain humble at all times I am deeply indebted to my fellow students who made the 5½ years pass quickly.

Finally, none of this work would have been possible without the love and support of my wife Adria.

TABLE OF CONTENTS

TABLE OF CONTENTS--Continued

LIST OF ILLUSTRATIONS

LIST OF ILLUSTRATIONS--Continued

LIST OF ILLUSTRATIONS--Continued

LIST OF TABLES

ABSTRACT

Speckle noise is an integral part of any laser projection display because it is the nature of laser (coherent) illumination to form interference patterns with high visibility. The granularity of the image due to the speckle formed on the viewer's retina degrades the image quality, thus stimulating the need for speckle reduction techniques applied to laser displays. An instrument to measure image plane speckle contrast was built based on a linear CCD detector array interfaced to an LSI-11 microcomputer. Speckle reduction techniques were then evaluated by comparing the contrast obtained with each method.

The effect of the spatial frequency response (MTF) on the measured contrast was studied, along with the statistical significance of the measurement which is limited by the finite sample space of 1024 detector pixels per CCD frame. The lowering of the contrast due to the array MTF can be minimized by working at extremely high F numbers (> 100). The sample space can be widened by taking more than one frame of data and treating all the frames as a single data set.

Techniques to reduce speckle noise in laser displays fall into two broad categories: reducing the coherence of light forming the speckle, and incoherently adding multiple uncorrelated (or partially correlated) speckle patterns. The first technique (effective only for monochromatic displays) was implemented by coating a screen with various dyes, phosphors, or fluorescent paints. Using the 514 nm line from an Argon

laser, the contrast can be reduced by almost 30% by spraying a thin layer of fluorescent paint on the screen. More speckle reduction can be achieved with an accompanying loss in image brightness.

The second technique involved creating a multiplicity of partially correlated speckle patterns that appear from the same position on the screen over the integration period of the eye. The different speckle patterns are produced by changing the angle of illumination while keeping a portion of the laser spot focused on the same point on the screen. The scan angle method (applicable to multi-color displays), can be implemented by properly synchronizing an acousto-optic modulator with the scan optics, and imaging the modulator on the screen. Using a beaded screen and a reasonable laser dither of 10 millirads, the contrast can be reduced by half.

CHAPTER 1

INTRODUCTION

The grainy, chaotic light distribution called speckle is familiar to anyone who has viewed the scattered light obtained by shining an ordinary helium-neon laser on a wall or a piece of paper. Speckle can also be observed as an annoying artifact in holograms of diffuse objects. White light speckle can be observed by looking at sunlight diffracted from a fingernail while squinting. A comparison of the speckle from a helium-neon laser with white light speckle leads to the fundamental observation that the clarity of a speckle pattern depends upon the spectral purity of the source. The term "speckle contrast" is a quantitative measure of the development of the speckle patterns or the amount of speckle noise present.

This dissertation is concerned with (1) the problems of measuring speckle contrast using charge coupled device (CCD) detector arrays, (2) the performance of an instrument based on a CCD detector array, and (3) application of the instrument to evaluate techniques for obtaining speckle contrast reduction in laser projection displays.

In this introductory chapter we give a historical overview of the development of the work contained in this dissertation and attempt to show where it fits in with previous research. The physics of image plane speckle formation and the first order statistics of fully developed speckle patterns are also reviewed.

Historical Overview

This dissertation grew from a contract with the Naval Training and Equipment Center (NTEC) in Orlando, Florida, to develop techniques for speckle contrast reduction in laser displays. A pilot simulator had been built at NTEC in which an image is painted on a large screen by an intensity modulated argon laser that is scanned in two dimensions. Because the display is projected by a laser, the Navy was interested in speckle reduction techniques, and also in methods of increasing the gain of their projection screens to increase the brightness of the dim image.

After the initial phase of work on this contract in which we suggested techniques for speckle reduction, we began to use a 128 pixel Reticon photodiode array to measure laser speckle contrast. It is clear in hindsight that the speckle patterns from screens in this early work were not being resolved by the photodiode array, and that this array did not possess the sensitivity required to measure the contrast from screens.

This problem directed us to investigate the signal-to-noise problems inherent in measuring contrast with detector arrays, as all previously reported measurements of image plane speckle were made with photomultiplier tubes. We decided that an instrument could be built using a charge coupled array, and we proceeded to build one based on a Fairchild 131 linear CCD array interfaced to an LSI-11 microcomputer.

The first measurements with this instrument showed that the average contrast from a monochromatic, polarized, speckle pattern was slightly less than one (the theoretical contrast is one), and more disturbingly, that there was an almost 40% variation in the contrast

measured from different sections of the same ground glass. These results led to the study of the probability density function of the contrast as a function of speckle number and of the measured contrast degraded by the modulation transfer function (MTF) of the array. This work is found in Chapter 2.

After the instrument was built, but concurrent with the theoretical work of Chapter 2 and the experimental verification of this work (Chapter 4), we studied techniques for reducing speckle contrast in laser scanned displays. The first attempts were to coat the projection screens with a dye, phosphor, or paint that would increase the spectral bandwidth (and thus decrease the coherence length) of the light returned to the viewer's eye. The advantage of this method is that it is cheap and simple to retrofit to any system already built or designed. The disadvantages of the coating method are that it is not applicable to multicolor displays and that the brightness of the image, for all of the materials we tested, would be reduced.

In the spirit of quick and simple, rather than making an exhaustive search and fine tuning of materials and methods, we tested commercially available dyes (in film form from the 3M Company), phosphors (from GTE Precision Materials and the Harshaw Chemical Co.), and locally available fluorescent spray paints. These materials were applied to the screens following the procedures recommended by the manufacturer. This work is described in Chapter 5.

Better optical techniques exist for speckle reduction in laser displays. These techniques primarily rely upon time multiplexing more

than one uncorrelated (or partially correlated) speckle pattern in the 1/30th of a second integration time of the viewer's eye. These scanning techniques are discussed in Chapter 6.

Chapter 7 contains a discussion of high-gain holographic screens. While not related to speckle reduction, this work presents a possible solution to increasing the brightness from front projection screens, and so fits into the general topic of laser displays.

This work on speckle reduction joins an already established body of literature on speckle reduction in holography and other areas that employ lasers for image projection or recording. The work on the performance of a CCD array for measuring contrast, and the probability density function of the contrast, are useful for discussing the accuracy of the measurements made on speckle reduction techniques.

Image plane contrast has been measured previously only by scanning the speckle in the image or defocused image plane with a photomultiplier tube (PMT). The reasons for using PMTs, which are explained in detail in Chapter 3, are primarily the high sensitivity and dynamic range necessary for resolving the speckle pattern. CCD technology opens the door to achieving close to PMT performance from a solid-state imaging detector. One area which I feel will benefit from this new technology is surface roughness measurements using image plane speckle contrast. The work in Chapters 2 and 4 is particularly relevant to this application.

The next section of this introductory chapter contains a historical overview of previous work in speckle reduction and previous

measurements of image plane speckle. The final section in Chapter 1 is a review of the first order statistics of monochromatic, polarized laser speckle.

Speckle Reduction Techniques

The earliest research in speckle, performed primarily by holographers, falls into the category of speckle reduction. Their interest was to eliminate (or at least reduce) the speckle in holograms, which is disturbing to an observer. An example of this early work is the technique of Leith and Upatniecks (1968) who placed a phase grating in the plane of the transparency in order to create several signal terms of differing angular spread. This technique preserves the redundancy of the hologram, but it does not work for holograms of diffuse objects. The tradeoff is between the amount of redundancy and the amount of speckle in the recorded hologram.

Other methods for reducing the speckle noise in holograms are to decrease the temporal coherence of the reconstruction beam, to decrease the spatial coherence of the reconstruction beam, and to average several speckle patterns together over the integration time of the observer. All of these methods are different ways of creating a speckle pattern that is the sum of more than one independent, or partially correlated, speckle pattern. This sum may be over wavelength, space, or time diversity.

For example, George and Jain (1972) studied speckle reduction in a microscope imaging system as a function of the wavelength spread necessary to decouple the polychromatic speckle. Cronin and Smith (1973) created a monochromatic spatially incoherent source by passing a laser

through a rotating prism, which caused the source to appear as an extended ring source. Dainty and Welford (1971) suggested relaying the reconstructed image from a hologram to a second image plane, and then continuously moving a sub-aperture in the pupil plane of the imaging lens. In this method the effective aperture creating the final image is reduced, so there is an accompanying loss in resolution and brightness. A review of the mathematical formalism of speckle reduction and methods for speckle reduction can be found in "Speckle Reduction" by T. S. McKechnie (1975) in Laser Speckle and Related Phenomena (ed. J. C Dainty).

Of more current interest than speckle reduction in holograms is speckle reduction for optical systems in which lasers are used for image formation. The use of a rotating or moving ground glass plate at the image plane of an interferometer to reduce speckle is well known. Lowenthal and Joyeax (1971) and Rawson et al. (1976) have discussed the much greater reduction in speckle by using two diffusers and moving one with respect to the other. Part of this dissertation will be concerned with reducing speckle noise in laser displays. Because the diameter of the laser spot on the screen is often larger or about the same size as the object plane point spread function of the observer's eye, the speckle pattern is not washed out by the scanning motion of the beam. Just as in holography, the speckle is an objectionable artifact of the laser creating the image.

Another area of interest is speckle reduction of images recorded in coherent light, such as by a laser radar (LIDAR) system. Dainty (1971) and George et al. (1976) have discussed the detection of objects

in images that are degraded by speckle noise. Lin and Wawah (1981) have discussed digital post-processing of images to reduce speckle in LIDAR systems. In this case the speckle is caused by laser scatter from a rough target (rough compared with the laser wavelength, usually 10.6 μm), and by atmospheric turbulence. Another area of interest is the effect of speckle on coherent adaptive optical (COAT) systems (Pearson et al., 1976).

A final, somewhat different, area of current interest is speckle reduction in multi-mode optical fibers (Rawson and Goodman, 1980; Epworth, 1981). Since the path traveled by each mode in a multi-mode fiber is different, there is a phase difference between the electric fields in different modes. The interference between these coherent but de-phased modes (a speckle pattern often called modal noise) may degrade the bandwidth of a particular optical fiber.

Surface Roughness Measurements

While a great deal of research in speckle has been devoted to ways for suppressing speckle, the flip side of the coin has been to harness speckle to provide information about physical systems. One of the methods proposed has been to measure the image plane contrast formed by a partially developed speckle pattern. Sprague (1972) used a PMT to measure polychromatic speckle contrast in a defocused image plane, and correlated this against RMS surface roughness. Asakura (1978) has done extensive research on using the contrast of monochromatic image plane speckle patterns to obtain the roughness of surfaces. His instrument uses a stationary PMT and an x,y stage to scan the speckle pattern, typically making 65,556 measurements per image. Goodman (1975),

Pedersen (1974), and others have developed models for contrast vs surface roughness.

Speckle techniques yield the root-mean-square surface height as a function of contrast as opposed to optical profilometers, FECO interferometers, or stylus devices, which return information on the detailed surface structure. Speckle measurements therefore give considerably less detailed information than these other devices. It is possible, however, that this average surface roughness parameter may be more valuable in some manufacturing or industrial areas than the detailed surface information. In these areas, the immunity to noise, environmental effects, and rough handling, and the fast data input afforded by CCDs would be required.

First Order Statistics of Laser Speckle

The first order statistics of monochromatic, polarized speckle patterns is the starting point for understanding laser speckle. Speckle formed with unpolarized or polychromatic light, or the speckle patterns formed by incoherently averaging more than one speckle pattern, can be conceptualized as the sum (in time, wavelength, or space) of simple, monochromatic, polarized speckle patterns. This section, which is included for completeness, is a review of the physics of speckle formation in the image plane of a lens, and of some of the first order statistics of speckle. All of the theory explained here is considered in detail in what has become the standard reference, "Statistical Properties of Laser Speckle," by J. W. Goodman (1975) in Laser Speckle and Related Phenomena

(ed. J. C. Dainty). The reader is also referred to an excellent review article, "Fundamental Properties of Speckle," by Goodman (1976).

Speckle Formation and Statistics

Consider points A and B in the object plane of Figure 1.1, illuminated by polarized, monochromatic light. If these points are sufficiently close to one another, the electric field amplitude spread function of each will partially overlap in the image plane, producing a beat in the resultant electric field. The irradiance in the image plane in the vicinity of the overlapping spread functions will be

$$I = |E_a + E_b|^2 = |E_a|^2 + |E_b|^2 + 2|E_a E_b| \cos\left(\frac{2\pi}{\lambda} \mathrm{OPD}\right) \qquad (1.1)$$

where the OPD is the optical path difference between the two fields.

If the amplitude spread function of the lens is large enough, the contribution to the total electric field will be made up of light from many elementary scattering areas, each with a different surface height. The sum of the interference terms between all elementary scattering areas and all other elementary scattering areas gives rise to the chaotic intensity pattern called speckle. This sum of amplitudes in the image plane can be thought of as a sum of phasors in the complex plane. Each component of the electric field has a phase an an amplitude, and the resultant electric field is found by the phasor addition (head to tail) of all the phasors at the image.

Goodman then makes the following two assumptions about the contributions from each elementary scatter:

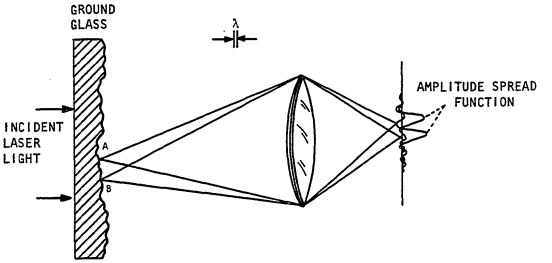

Fig. 1.1. Speckle formation in the image plane of a lens.

1) the magnitude and the phase of the electric field from any one scattering area are unrelated to each other, and to the phase and amplitude of the electric field from all other scattering areas, and

2) the surface is rough compared to the wavelength of illumination, so the phase excursions ($2\pi OPD/\lambda$) of the different phasors will be many times 2π. This assumption leads to a uniform distribution of phases between 0 and 2π. The speckle formed by monochromatic, polarized light under these two assumptions is termed a fully developed speckle pattern.

With the above assumptions, the problem becomes mathematically identical to the canonical random walk in a complex plane. The classical analogy is that of a drunk at a light post. Given that the drunk is equally likely to turn in any direction, and that the size of the step he takes is independent of the direction, after M steps how far from the light post will he be, and in what direction will he be facing? (The answer is, of course, that he will most likely be back at the light post.)

The results of the random walk problem, provided that the number of scattering centers contributing to the summation is very large, are that the probability density function of the irradiance, P(I), is

$$P(I) = \frac{1}{\langle I \rangle} \, e^{-I/\langle I \rangle} \quad , \tag{1.2}$$

where $\langle I \rangle$ is the ensemble average irradiance. The second moment is then

$$\langle I^2 \rangle = \int I^2 P(I) dI = 2 \langle I \rangle^2 \quad . \tag{1.3}$$

The contrast of a speckle pattern is defined as the standard deviation of the irradiance divided by the ensemble average irradiance. For the fully developed speckle pattern whose statistics are determined by Eqs. (1.2) and (1.3), the contrast (Eq. 1.4) becomes one

$$C = \frac{(\langle I^2 \rangle - \langle I \rangle^2)^{\frac{1}{2}}}{\langle I \rangle} = 1 \quad . \tag{1.4}$$

For a uniform irradiance distribution with no speckle, there are no fluctuations in the irradiance, so the standard deviation and the contrast are 0. For a speckle pattern that is less severe than a fully developed speckle pattern, the contrast will be between 1 and 0. Thus contrast is a measure of the amount of speckle in an irradiance distribution.

Contrast plays a role analogous to fringe visibility in interferometry. On a fundamental basis, contrast and visibility are both measures of the coherence of the interfering light. In an interferometer, perfect coherence and beam balance give a visibility of 1. In a speckle pattern, perfect coherence and completely randomized phase distributions yield a contrast of 1. (It is interesting to note that a fringe pattern of visibility 1 has a contrast of 0.7.)

Another parameter of interest is the power (or Wiener) spectra of the speckle pattern in an image plane. This function is needed to calculate the effect of the spatial frequency response of the detector array on the measured speckle contrast. If we consider points A and B in the aperture of Figure 1.2, this pair of points will contribute to the spatial frequency $u=d/\lambda z$ only. Thus for a fixed focal length lens, the power

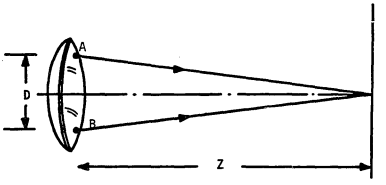

Fig. 1.2. Speckle frequency formation in the image plane of a lens.

spectra at a specific spatial frequency can be thought of as the number of points in the aperture with separation d. The cutoff frequency is determined by the maximum distance between points in the aperture, which is from points diagonally opposite each other at the edges of the aperture.

This number density of correlated points is equivalent to the autocorrelation of the aperture, which is the diffraction limited incoherent optical transfer function of the lens. The power spectra, Fig. 1.3, can thus be shown to equal (Goodman, 1975)

$$w(u,v) = \frac{8\lambda^2 F\#^2}{\pi^2} \left\{\cos^{-1}(\lambda F\#\rho) - (\lambda F\#\rho)\left(1-(\lambda F\#\rho)^2\right)^{\frac{1}{2}}\right\} + \delta(u,v) \ . \tag{1.5}$$

A final property of interest is the contrast reduction by incoherently summing more than one speckle pattern with the same statistics. As pointed out by Goodman (1976), summing M uncorrelated, real valued, random variables yields a random variable whose mean and variance are M times the mean and variance of the original random variable. If the original contrast is C_o the reduced contrast due to the uncorrelated sum becomes

$$C = \frac{M^{\frac{1}{2}}}{M} \ C_o = \left(\frac{1}{M}\right)^{\frac{1}{2}} C_o \ . \tag{1.6}$$

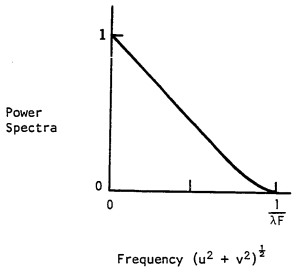

Fig. 1.3. Image plane speckle power spectrum.

CHAPTER 2

SPECKLE CONTRAST MEASURED WITH A DETECTOR ARRAY: THEORETICAL CONSIDERATIONS

The design of a speckle contrast measuring instrument using a detector array is a balance between two opposite requirements. At one extreme is the desire to measure a slowly changing (with respect to the pixel spacing) speckle pattern--one with few speckles across the array--to reduce the effects of high spatial frequency filtering by the detector array. At the other extreme is the need to measure a rapidly changing speckle pattern--one with many speckles across the array--to increase the statistical significance of the measurement. The key parameter is the F-number (abbreviated as F#) of the imaging lens, which fixes the spatial frequency band limit of the speckle pattern and the average speckle size. In addition, fixing the F# determines the image plane irradiance and consequently, detector parameters such as integration time and signal to noise ratio.

In this chapter we discuss three factors that must be considered when designing an instrument for measuring speckle contrast: sampling, truncation of the data set, and image plane irradiance. A fully developed speckle pattern is used as the input speckle field because the statistics are well known and exist in closed form. We argue that using such a field is a worst case analysis, and show that the limiting uncertainty arises from truncating the data set.

Sampling

Measuring any irradiance distribution with a detector array requires that the sampled, digitized data bear an excellent resemblance to the real, continuous distribution. Since the diameter of the smallest speckle in a fully developed speckle pattern is $1.22\lambda F\#$, if the F# of the imaging lens is made sufficiently large, all speckles will be larger than each individual pixel of length p. If the pixels are contiguous, the sampled pattern will, intuitively, be a "good" copy of the real pattern.

This problem is best analyzed in terms of the modulation transfer function, MTF, of the detector array, and the power spectra, W, of the speckle pattern. A solution for sampling using a circular lens aperture and a circular detector pixel has been discussed by Dainty (1970), and for a square detector pixel and square aperture by Gerritson, Hannan, and Ramberg (1968). Goodman (1975) has developed the first order statistics for integrated, and blurred speckle, and has evaluated the number of correlation cells (equal to the contrast^{-2}) for the case of a Gaussian irradiance profile and a square detector pixel. Barakat (1973, 1978) and Scribot (1974) have also studied the effects of a finite size aperture on the first and second order speckle statistics.

We evaluate the contrast for a circular aperture and a linear detector array with square pixels following the approach of Dainty (1970), assuming constant irradiance in the object plane. We consider first the case of the transfer function degraded by the finite sized detector pixels, the ideal CCD MTF, and then further reductions in the transfer

function because of charge-transfer inefficiency, and photo-electron diffusion. The total MTF becomes the product of the individual MTF's.

Ideal CCD MTF Case

To calculate the contrast reduction due to spatial averaging of the signal over the pixel shape in terms of the MTF, the power spectra of the signal from the detector array, W_d, is found as the product of the speckle pattern power spectra incident on the array and the square of the MTF. The variance of the signal from the array can be shown to be the integral of W_d over all frequencies. Provided that W is correctly normalized, the measured speckle contrast is the square root of the signal variance.

The power spectra for image plane speckle has been shown to equal the modulation transfer function of a lens in incoherent light (Goodman, 1975). For a circular aperture, the speckle power spectra W is given by

$$W(u,v) = \frac{8\lambda^2 F\#^2}{\pi^2} \left[\cos^{-1}(\lambda F\#\rho) - (\lambda F\#\rho)\left(1-(\lambda F\#\rho)^2\right)^{\frac{1}{2}}\right] + \delta(u,v) \quad , \tag{2.1}$$

where

u,v = x,y transform spatial frequency coordinates

$\rho = (x^2 + y^2)^{\frac{1}{2}}$

λ = wavelength of light

F# = effective f-number of the imaging lens

and the power spectrum is normalized to unity irradiance.

The autocorrelation function, $R(x_o,y_o)$, is the Fourier transform of the power spectra (Weiner-Kirtchen theorem: see Frieden, 1980), given by

$$\langle I(x+x_o,y+y_o)\ I(x,y)\rangle = \int_{-\infty}^{\infty}\int_{-\infty}^{\infty} e^{2\pi i(ux_o+vy_o)}\ W(u,v)dudv. \quad (2.2)$$

Setting $x_o = y_o = 0$, one finds the second moment of the irradiance as

$$\langle I^2(x,y)\rangle = \int_{-\infty}^{\infty}\int_{-\infty}^{\infty} W(u,v)dudv\ . \quad (2.3)$$

The effect of a finite size detector element is to integrate the speckle over the pixel length, perhaps with some weighting function. This is equivalent to filtering in the spatial frequency domain. The effect of this filtering on the power spectra of the signal from the detector can be shown to be (Papoulos, 1965)

$$W_d(u,v) = [MTF(u,v)]^2\ W(u,v)\ . \quad (2.4)$$

The ideal MTF of a CCD detector is just the Fourier transform of the pixel shape (Barbe and Campana, 1977). For contiguous, square, pixels, the MTF becomes

$$MTF(u,v) = \mathrm{sinc}(px)\mathrm{sinc}(py)\ , \quad (2.5)$$

where p is the length of the square pixel and we have used Gaskill's (1978) definition of the sinc function. The average irradiance $\langle I\rangle$ is unchanged by the filtering operation of the array. Thus substituting Eqs.

(2.1) and (2.5) into Eq. (2.4), and the resulting expression for W_d into Eq. (2.3), yields an expression for the constrast, C, as

$$C^2 = \frac{8\lambda^2 F\#^2}{\pi^2} \int_0^1 \int_0^1 [\cos^{-1}(\lambda F\#\rho) - (\lambda F\#\rho)\left(1-(\lambda F\#\rho)^2\right)^{\frac{1}{2}}]$$

$$\cdot \operatorname{sinc}^2(pu)\, \operatorname{sinc}^2(pv) du dv \quad . \tag{2.6}$$

Letting $\eta=\lambda F\#u$, $\xi=\lambda F\#v$, and $\gamma=p/\lambda F\#$, Eq. (2.6) can be rewritten as

$$C^2(\gamma) = \frac{8}{\pi^2} \int_0^1 \int_0^1 \cos^{-1}(\xi^2+\eta^2)^{\frac{1}{2}} - (\xi^2+\eta^2)^{\frac{1}{2}}\left(1-(\xi^2+\eta^2)\right)$$

$$\cdot \operatorname{sinc}^2(\gamma\xi)\, \operatorname{sinc}^2(\gamma\eta)\, d\xi d\eta \quad . \tag{2.7}$$

The term γ is proportional to the band limit of the speckle pattern divided by the sampling rate of the array. (Equivalently, γ is proportional to the ratio of pixel length to speckle diameter.) For $\gamma=0$ ($p=0$), the detectors have zero area, and the contrast should equal one. For increasing γ (i.e., for increasing pixel length), more averaging of the speckle pattern occurs for a fixed lens aperture and the contrast is lowered. The Nyquist frequency is reached when the inverse of twice the sampling interval equals the maximum spatial frequency of the speckle pattern, or

$$\frac{1}{2p} = \frac{1}{\lambda F\#} \tag{2.8}$$

Thus $\gamma=1/2$ at the Nyquist frequency.

A similar equation for the contrast as a function of γ can be written for a circular aperture (Dainty, 1970). Substituting somb(pu) for the MTF of the detector in Eq. (2.5), changing to polar coordinates and integrating over the angular dependence, the contrast can be written as

$$C^2(\gamma) = \frac{64}{\pi} \int_0^1 \left(\cos^{-1}(z) - z(1-z^2)^{\frac{1}{2}}\right) \text{somb}^2(\gamma z) z dz \qquad (2.9)$$

where

$$z = (\xi^2+\eta^2)^{\frac{1}{2}} \quad .$$

Equations (2.7) and (2.9) can be integrated numerically for difference values of γ, and the results are shown in Figure 2.1. It is interesting to note that the contrast drops off slightly faster for square pixels of length p than it does for circular pixels of radius p/2, because the area of the square pixels is larger.

MTF - Charge Transfer Inefficiency

During the transfer of charge along a CCD shift register some portion of the charge, ε, is lost from every charge bucket at each transfer. This lost charge is subsequently added to the next sample moved into its potential well, and has the effect of smearing the image. The MTF due to this transfer inefficiency for a linear CCD shift register with β transfers at spatial frequency u is (Barbe and Campana, 1977)

$$(\text{MTF})_{\text{transfer}} = e^{-\beta\varepsilon\left(1-\cos(2\pi pu)\right)} \; e^{-i\beta\varepsilon\sin(2\pi pu)} \qquad (2.10)$$

Using the substitutions of the previous section, the term of interest, $|\text{MTF}|^2$, can be written as

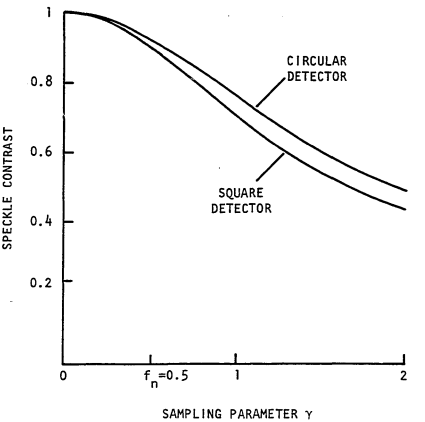

Fig. 2.1. The effect of the finite size detector pixels on speckle contrast for circular and square pixels.

f_n is the Nyquist frequency.

$$|(\mathrm{MTF})_{\mathrm{transfer}}|^2 = e^{-2\beta\varepsilon\left(1-\cos(2\pi\gamma\xi)\right)} \tag{2.11}$$

The effect of this additional term to the MTF on the contrast can be calculated by including Eq. (2.11) inside the integral of Eq. (2.7) and numerically integrating as done previously.

The CCD used in our experiment is a 2 phase device with two separate 516 pixel shift registers (i.e., β=516). The charge transfer inefficiency ε is typically 1×10^{-5}, and at worst 5×10^{-5}. The contrast calculated for these parameters is shown in Figure 2.2. It is evident that the degradation in contrast due to charge transfer inefficiency is small out to the Nyquist frequency.

MTF - Photoelectron Diffusion

The depth in the silicon substrate of the CCD at which an incident photon is absorbed and a photoelectron produced is a strong function of wavelength.

The farther from the depletion region the photoelectron is produced, the more likely it is that the photoelectron will migrate horizontally away from the proper potential well before being captured. This effect causes smearing of the image and a resultant loss in resolution.

The MTF due to diffusion is (Barbe and Campana, 1977)

$$(\mathrm{MTF})_{\mathrm{diffusion}} = \frac{\cosh(d/L_o)}{\cosh\left\{\frac{d}{L_o}\left[1+(2\pi u L_o)^2\right)^{\frac{1}{2}}\right\}} \tag{2.12}$$

where d is the distance away from the depletion region that the photons are absorbed, and L_o is the diffusion length in the silicon.

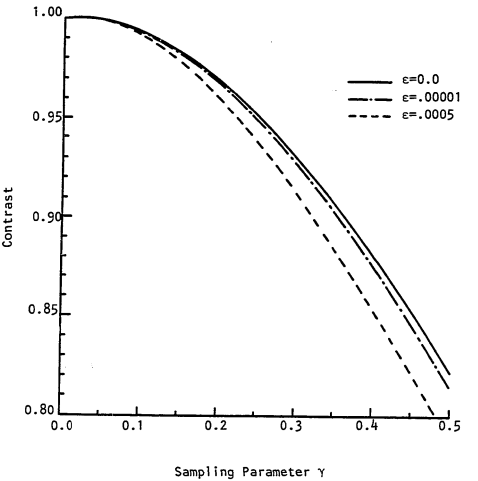

Fig. 2.2. The effect of a square pixel and charge transfer inefficiency on speckle contrast up to the Nyquist frequency.

β=516 corresponding to our 1024 element array.

Figure 2.3 shows the marked decrease in the MTF due to photoelectron diffusion as a function of wavelength. This data, which represents an average frequency response with wavelength, rather than Eq. (2.12), was used to calculate the contrast as a function of wavelength (Fig. 2.4) because the diffusion length, Lo, exhibits wide variability with each individual CCD (Dyke, 1981). For wavelengths shorter than 600 nm the effect of photoelectron diffusion is negligible.

There are two major implications of the wavelength dependent contrast. The first is that the contrast measurements of polychromatic speckle patterns with significant power at wavelengths longer than 700 nm will contain a subtle error due to the color sensitive spatial frequency response of the CCD. The second is that contrast measurements made with sources whose wavelength is greater than 800 nm will require extremely large F#'s (> 200) to adequately sample the speckle pattern. While the responsivity of the CCD increases approximately linearly for $\lambda \lesssim 1$ μm, the sampling parameter γ decreases approximately linearly for $\lambda \gtrsim 600$ nm. Since the power in the image plane is proportional to γ^{-2}, the linear increase in sensitivity is not enough to offset the quadratic decrease in power.

Discussion of the Sampling Requirement

The theoretical contrast of a completely developed speckle pattern is 1.0. The contrast measured by any experimental apparatus will be less than 1 due to spatial resolution limitations of the detector. Ultimately we are interested in measuring speckle patterns of reduced contrast. Because the power spectra of these speckle patterns is also

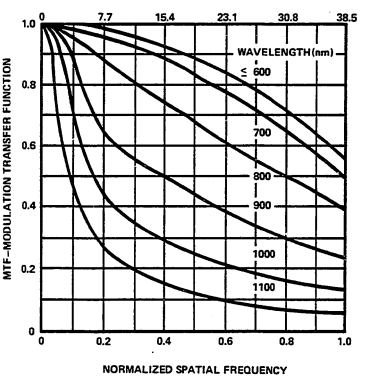

Fig. 2.3. MTF of a CCD vs wavelength.

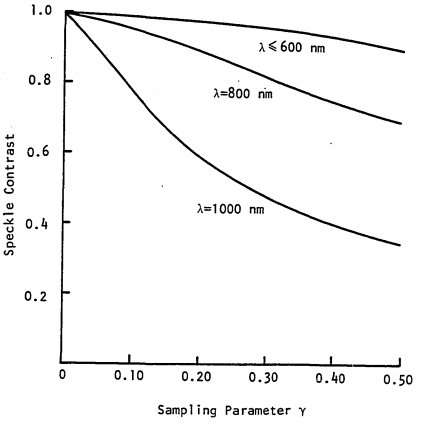

Fig. 2.4. The effects of photo-electron diffusion along with charge transfer inefficiency, and square pixel size on the measured contrast.

unknown, it is not possible to correct for the spatial resolution of our instrument. Therefore, the instrument should measure contrast with as little degradation as possible.

The spatial frequency response of linear CCD detector arrays is limited by the finite pixel size, charge transfer inefficiency, and photoelectron diffusion. We have studied the impact these have on the measured contrast of a fully developed speckle pattern. The conclusion is that for wavelengths less than 600 nm and sampling parameters, γ, less than .25 (which for pixel widths of 13 μm imply an F# $\gtrsim$ 100) the degradation of the contrast is less than 3%.

Statistical Uncertainty due to Data Truncation

The F# of the imaging lens used to form an image plane speckle pattern determines the spatial frequency band limit of the pattern. The F# is used to match the spatial frequency characteristics of the detector array to the speckle pattern. Fixing the F# for this purpose also determines the number of speckles intercepted by the array since the speckle diameter is $\approx 1.22\lambda F\#$.

The definition of contrast, C, Eq. (1.4), is in terms of an ensemble average which, by the usual assumptions of stationarity, can be equated to an average over an infinite number of data points. However, any laboratory experiment contains only a finite number of sampled points. This truncation of the number of data points used to experimentally compute C gives rise to some statistical spread for those measured values of the contrast.

Therefore, fixing the F# of the imaging lens not only determines the degradation of C due to sampling, but also determines the statistical uncertainty of the measurement. For a given number of data points we examine how large this statistical uncertainty is, and what its effect is on the average contrast.

Probability Density of the Contrast - Fully Developed Speckle

The measured contrast from M samples of the irradiance I is calculated as

$$\hat{C} = \frac{\hat{\sigma}}{\hat{I}} \tag{2.13}$$

where $\hat{\sigma}$ and $\hat{I}$ are calculated as

$$\hat{I} = \frac{1}{M} \sum_{j=1}^{M} I_j \tag{2.14}$$

and

$$\hat{\sigma}^2 = \left(\frac{1}{M-1}\right) \sum_{j=1}^{M} (I_j - \hat{I})^2 \quad . \tag{2.15}$$

(The character ^ implies a measured quantity. In statistics a measurement is often called an estimate.) The probability density of the irradiance for a fully developed speckle pattern is known (Goodman, 1975) as

$$P_I(I) = \frac{\exp(-I/\langle I \rangle)}{\langle I \rangle} \tag{2.16}$$

There are well established analytic techniques for finding the probability density of a given random variable (in this case $\hat{C}$) given its functional dependence on a second random variable of known probability density (I). While these techniques are straightforward, we were unable to find a closed form solution due to the complicated functional dependence of C on I, which can be written by substituting Eqs. (2.14) and (2.15) into Eq. (2.13) as

$$\hat{C} = \left(\frac{M}{M-1}\right)^{\frac{1}{2}} \left(\frac{M \sum_{j=1}^{M} I_j^2}{\left(\sum_{j=1}^{M} I_j \right)^2} - 1 \right)^{\frac{1}{2}} \tag{2.17}$$

B. Roy Frieden has pointed out that an analytic solution to this problem does exist, and will appear in Probability and Statistics in Optics, B. Roy Frieden, to be published by Springer-Verlag.

Instead of solving for $P_{\hat{C}}(\hat{C})$ from Eqs. (2.16) and (2.17), we performed a Monte-Carlo simulation. M independent values of the irradiance I were chosen from the probability distribution $P_I(I)$, and the speckle contrast was calculated from these values. This procedure was performed 100,000 times for one value of M to build up the statistics. $P_I(I)$ can be generated from a 0 to 1 random number generator which returns Y as (Frieden, 1980)

$$I = -\ln(1-Y) \tag{2.18}$$

where we have normalized for $\langle I \rangle = 1$.

The probability density for the expected value of the measured contrast, $P_{\hat{C}}(\hat{C})$, is shown in Figure 2.5 for several values of M. The

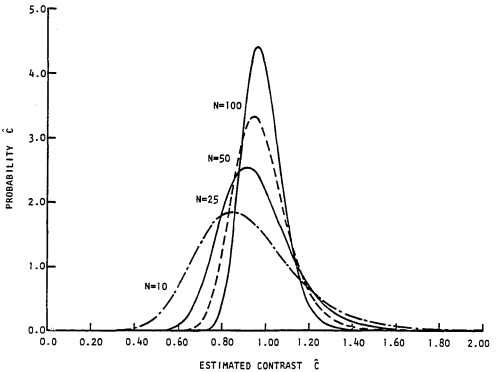

Fig. 2.5. Probability density of the contrast as a function of the number of independent sampled data points.

effects of using a limited number of data points to calculate C are that the standard deviation of the contrast, $\sigma_{\hat{C}}$, becomes increasingly larger for smaller M (approximately as $(1/M)^{\frac{1}{2}}$), and that the average contrast becomes increasingly smaller than 1 for decreasing M.

Speckle Number

In the previous section we have simulated the probability density of the contrast as a function of the number of independent, sampled data points used to calculate the contrast. The number of pixels illuminated by a speckle pattern is not equal to the number of independent sampled data points because the sampled irradiance values within each speckle are partially correlated, not independent. The autocorrelation function, A(r), for image plane speckle is shown by Goodman (1975) to be

$$A(r) = 1+\text{somb}^2(r/\lambda F) \tag{2.19}$$

The diameter of each speckle, $1.22\lambda F$, is determined by the first zero of the sombrero function. We model the number of independent irradiance measurements within a speckle pattern by assuming that:

1. all irradiance measurements made within one speckle diameter are completely correlated.
2. all irradiance measurements made more than one speckle diameter apart are uncorrelated.

The first approximation underestimates the amount of information within a detector frame because sampled points within each speckle are only partially correlated, rather than completely correlated. The second approximation underestimates the amount of information with a

detector frame because there is some degree of correlation between adjacent speckles.

With N_p and γ defined in the previous section, the number of independent irradiance measurements in a single detector frame, M, is thus given by the length of the detector array divided by the speckle diameter, or,

$$M = \frac{N_p P}{1.22\lambda F\#}$$

$$= \frac{\gamma N_p}{1.22} \tag{2.20}$$

Table 2.1 lists M for arrays with standard pixel numbers, for $\gamma = 0.5$, and $\gamma = 0.25$. The corresponding $\sigma_{\hat{C}}$ for a given M is plotted in Figure 2.6. It is evident that the portion of the curve that bends is the most profitable to operate upon because past this bend there is a smaller decrease in $\sigma_{\hat{C}}$ for a large increase in N_p.

From Eq. (2.17) and the central limit theorem, $P_{\hat{C}}(\hat{C})$ can be expected to be roughly Gaussian. (The plots of $P_{\hat{C}}(\hat{C})$ in Figure 3.4 do appear to be Gaussian.) Therefore $\sigma_{\hat{C}}$ can be roughly interpreted as having the same confidence interval as for a Gaussian probability distribution. Approximately 68% of the measurements should fall within $\sigma_{\hat{C}}$, and 96% within $2\sigma_{\hat{C}}$.

For the 1024 element array used in our experiment, M=210 at $\gamma = 0.25$, and $\sigma_{\hat{C}} = 6.7\%$. (The position for M=210 is indicated by a circle in Figure 2.6.) If the 2.5% degradation due to sampling is included, we expect 68% of the contrast measurements from a single detector frame to be $C = 0.97 \pm 0.04$ and 96% to be ± 0.07.

Table 2.1. The average value and standard deviation of the contrast for two values of γ, for standard pixel length arrays.

Array Size N_p	Sample Size N	γ	$\bar{\hat{C}}$	$\sigma_{\hat{C}}$
128	21	.25	.958	.183
256	42	.25	.977	.139
512	84	.25	.987	.103
1024	168	.25	.995	.074
2048	336	.25	.997	.053
128	52	.5	.981	.127
256	105	.5	.992	.093
512	210	.5	.995	.067
1024	420	.5	.998	.049
2048	839	.5	.999	.033

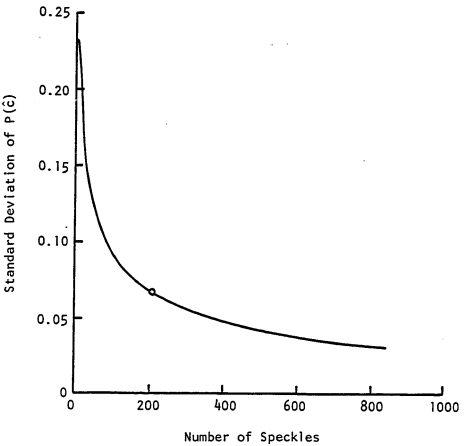

Fig. 2.6. The standard deviation of the contrast determined by the number of speckles intercepted by the array.

The circle marks the nominal operating point with our 1024 element array.

In Chapter 3 the instrumental uncertainty for each measurement are shown to be less than the uncertainty calculated above. Thus the limiting uncertainty in single frame measurements is the statistically small sample space.

Probability Density of Contrast -
Partially Developed Speckle Patterns

We expect that the uncertainty introduced by using a limited sample space to calculate the contrast for a partially developed speckle pattern will be less than the uncertainty introduced for a completely developed speckle pattern (i.e., the width of the curves in Figure 2.4 will be decreased if the speckle pattern has been formed with partially coherent light, or if it has been temporally or spatially averaged). Since the uncertainty of the experiment is limited by this truncated sample space, the uncertainties in a fully developed speckle pattern are the limiting case for a partially developed speckle pattern.

A partially coherent source can be split into the sum (in irradiance, not field) of a completely coherent source and a completely incoherent source. The fraction of irradiance of the coherent source to the total irradiance is determined by the complex coherence function (Born and Wolf, 1975, p. 503). Fluctuations in the average irradiance and fluctuations in the standard deviation of the irradiance give rise to fluctuations in the contrast. Since there will be no fluctuations in these quantities from the incoherent part of the partially coherent source, the total fluctuations in the contrast will be reduced for a partially developed speckle pattern.

Detector Plane Irradiance

Once the F# of the imaging lens has been determined by sampling requirements and constraints on statistical fluctuations in the contrast, the image plane irradiance, E (watts/m^2), can be computed from

$$E = \frac{L}{4F\#^2}$$

$$= \frac{\gamma^2 \lambda^2 L^2}{4p^2} \qquad (2.21)$$

where L is the object plane radiant exitance. We have assumed 1-to-1 imaging, and a perfect Lambertian scatterer.

Substituting λ = 0.5 μm, p = 13 μm, and γ = 0.25 into Eq. (2.17), the image plane irradiance will be 10^{-5} times smaller than the object plane radiant exitance. With typical CCD detector array responsivities of about 1 V/μJ-cm^2, the saturation times will be about 300 ms using a 250 mW Argon laser. While this is a relatively long exposure for a CCD, a reasonable signal-to-noise ratio can be achieved using the subtraction and averaging techniques described in Chapter 3.

CHAPTER 3

INSTRUMENTATION

This chapter describes the speckle measuring instrument. The first section explains the advantages and disadvantages of measuring speckle contrast with a CCD array and compares CCDs with other detectors suited for this purpose. The video and the interface electronics are described in the next section. The third, fourth, and fifth sections treat cooling the array and laser power monitoring, software, and multiple reflections from the CCD window, respectively. The last section explains the instrumental sources of error.

Figure 3.1 (a & b) is a photograph of the instrumentation. Figure 3.2 is a block diagram. The system is based on a DEC LSI-11 micro-computer and a Fairchild 131, 1024 pixel, buried channel linear CCD array. The computer is used to control the CCD and to collect data. It also serves as a processor to compute statistics, and to manipulate, store, and display data. Additional hardware connected to the LSI-11 includes a 12-bit A to D converter, a 12-bit D to A converter, two half megabyte floppies, a CRT terminal, a remote stage, a laser shutter, a plotter, and a Versatec printer.

The light from an argon laser operating single mode at 514 nm is spatially filtered, collimated, and focused on or through the surface under study. A shutter is placed after the exit aperture of the laser and is opened or closed by the computer for digitizing either a data

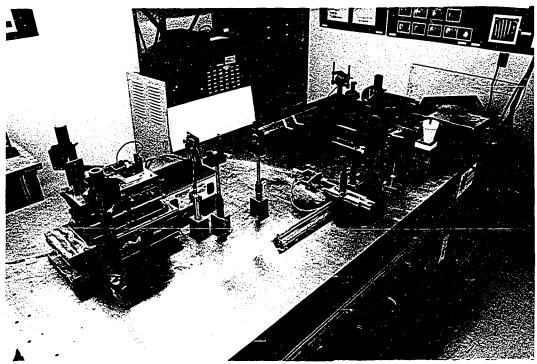

(a)

Fig. 3.1. Speckle contrast measuring instrument.

(a) Optics for measuring the contrast of screens.

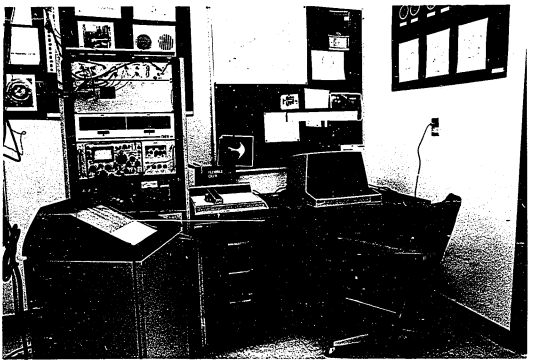

(b)

Fig. 3.1.--Continued

(b) Computer and peripherals of the contrast instrumentation.

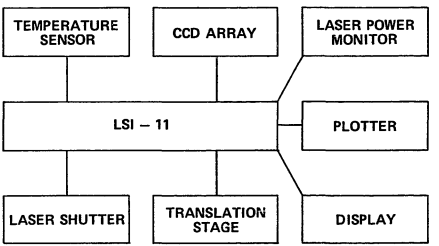

Fig. 3.2. Block diagram of the speckle measuring instrument.

frame or a dark noise frame. The speckle contrast is calculated for each 1024 pixel frame or from a larger data set made by stepping the movable stage containing the sample under study. The operating software allows for a real-time display of the array, cataloging and retrieval of old data, plotting, compilation of irradiance or contrast statistics (in histogram form), or calculation of the speckle power spectra. Since the experiment is completely automated, all experimental parameters, such as integration times, number of data frames, etc., are entered from the terminal. When the microcomputer is not actively digitizing data from the CCD, the array temperature and laser power are updated every 150 ms.

Linear CCDs, Two Dimensional CCDs, Vidicons, and Photomultipliers

Traditionally, the statistics of speckle patterns have been measured using photomultiplier tubes (PMTs) as in Mckehine (1973), Sprague (1972), or Asakura (1978). Because small scan apertures are needed to resolve the speckle, whose diameter is half of the incoherent point spread function (PSF) of the imaging lens, the high-gain, low-noise characteristics of PMTs have been considered desirable. The major disadvantage of such systems is that some form of mechanical scanning is required to move the speckle pattern across the detector aperture. This requires an additional piece of hardware, and implies that the speckle pattern must remain stationary for comparatively long times. PMTs also suffer from problems common to vacuum tube technology; PMTs require well-regulated power supplies, they are sensitive to a large number of environmental effects, and they suffer from hysteresis under certain conditions.

Vidicons are also vacuum tube devices and so suffer from some of the above problems. However vidicons are imaging detectors, so no scanning is necessary. Thus they are potential candidates for measuring image plane speckle contrast.

CCDs are also imaging detectors and are immune to many of the problems that plague vacuum detectors. They are also candidates for measuring image plane speckle contrast.

In the following parts of this section we compare linear and two-dimensional CCDs with vidicons. While CCD technology is in its infancy, vidicon technology is almost 40 years old. As a result of this long history, there are many different types of vidicons such as Isocons, Orthocons, Plumbicons, SIT tubes, and SEC tubes, all with their own advantages and disadvantages. It would be unwieldy to inter-compare all these types of devices with CCDs. Therefore, the following comparisons are made between a typical 1-in silicon target vidicon tube and commercial Fairchild CCDs.

Dynamic Range

The typical dynamic range for silicon target vidicons is 6 bits (RCA Electro-Optics Handbook, 1972), whereas for uncooled CCDs it is about 8 bits. For every 8°C reduction in temperature, the noise from a CCD is reduced by half. Thus cooling a CCD with a thermoelectric cooler by 32°C will increase the dynamic range to 12 bits.

Pixel Widths

The number of resolvable points across one line of a vidicon scan is about 512 (RCA Electro-Optics Handbook, 1974), so the equivalent pixel width is 25.4 mm/512, or ≈ 50 μm. Pixel widths of 13 μm are currently available for linear CCDs, and 18 μm for two-dimensional CCDs. As discussed in Chapter 2, the F-number (F#) of the imaging lens will scale in proportion to the pixel width due to sampling requirements. Since the image plane irradiance (watts/m^2) is proportional to $1/F\#^2$, the irradiance incident upon a vidicon with a 50 μm resolution pixel must be reduced from the irradiance incident upon a linear array by $(13\ \mu m/50\ \mu m)^2$, or 92%. The same reasoning leads to a reduction of 52% for a two-dimensional CCD from a linear CCD.

Number of Resolvable Speckles

The number of resolvable speckles contained in each data set, N, was shown in Chapter 2 to determine the statistical accuracy of the measurement. Figure 3.3 clearly shows that, for an equal number of pixels, the number of speckles intercepted by the detector is smaller for a two-dimensional detector than for a linear detector. Figure 3.3 also shows that the number of speckles intercepted by a two-dimensional device, N2, diminishes as the sampling becomes finer.

N2 is given by the area of the detector divided by the area of each speckle. In Chapter 2 γ is defined as $p/\lambda F\#$, or proportional to the pixel width divided by the speckle size. For γ=0.5, the sampling is as coarse as possible without aliasing (i.e., the Nyquist limit). As γ approaches 0, the sampling becomes finer. Thus, with N_p equal to the

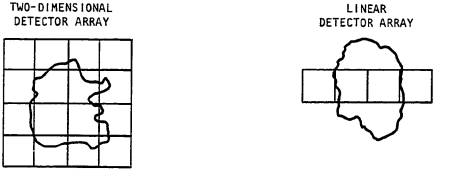

Fig. 3.3. Conceptual view of the number of speckles intercepted by a linear and two-dimensional CCD.

total number of pixels, N2 is given by

$$N2 = \frac{N_p p^2}{\pi \left[\frac{1.22\lambda F\#}{2}\right]^2}$$

$$= \gamma^2 N_p/1.17 \qquad (3.1)$$

The number of speckles intercepted by a linear array, N1, is the length of the array divided by the speckle diameter, or

$$N1 = \frac{N_p P}{1.22\lambda F}$$

$$= \frac{\gamma N_p}{1.22} \qquad (3.2)$$

A comparison of Eqs. (3.1) and (3.2) shows that for an equal number of pixels, with $0 \leqslant \gamma \leqslant \frac{1}{2}$, $N1 \geqslant 1.9\ N2$. As an example, consider sampling a speckle pattern with a 32 x 32 element (1024 total) two-dimensional array compared with a 1024 linear array. In this case N1=420, N2=219, and the reduction in the standard deviation of the contrast for the linear array over the two-dimensional array will be $\approx(219/420)^{\frac{1}{2}}$, or 0.7. A more realistic example would be to compare a 1024 linear array with a 512 x 512 vidicon operating at twice the Nyquist rate. In this case, the standard deviation of the contrast measured by the vidicon would be 8 times smaller than the contrast measured by the array, but at the expense of processing 256 times more data.

The conclusion to be reached is that unless the speckle does not have circular symmetry, or the precision of the contrast must be greater

than what can be achieved with the largest linear arrays (typically 2048 elements), a linear detector is preferable to a two-dimensional device.

Integration Time

A drawback of vidicons, unique to the problem of measuring image plane speckle with a vidicon, is the inability to easily adjust the light integration time on the photocathode. Normally the light falling on a vidicon tube is adjusted by varying the F# of the imaging lens. As discussed in Chapter 2, however, the F# is fixed by the constraints of spatial frequency sampling and is not a free parameter. To adjust the intergration time with a vidicon would require changing the electron beam scan time. This would be a difficult task for large changes because the target properties and the internal electronics are matched to the scan time. In a CCD the integration time is limited only in that it must be longer than the read-out time, and shorter than the saturation time. In addition, the exposure time can be decoupled from the array readout time for single frame measurements.

Electronics

The electronics needed to interface an RS-170 standard video signal with a small computer are complicated because of the high data bandwidth ($\sim$ 5 MHz) contained within the horizontal and vertical syncs. Usually a special-purpose frame grabber (A to D converter board) is needed to digitize video signals. Data from a CCD are received in serial at a preset clock rate, and it is relatively straightforward to directly interface this signal to a general-purpose A to D converter.

Summary

In summary, the advantages to using a linear CCD instead of a PMT, a two-dimensional CCD, or a vidicon are:

1. The CCD is an imaging device, so no mechanical scanning is necessary.
2. The CCD is a solid-state detector without many of the drawbacks of vacuum devices.
3. The number of speckles per pixel is greater for a linear detector than for two-dimensional detector arrays or vidicons.
4. CCDs have good sensitivity and medium spatial frequency response.
5. There is flexibility in determining integration times to match the irradiance of the source.
6. CCDs are comparatively simple to interface to a microcomputer.

CCD, CCD Board, and Interface Electronics

A block diagram of the CCD, a Fairchild model 131 buried channel linear array, is shown in Figure 3.4. The chip contains 1024 photo-pixels, eight non-valid pixels that precede the valid photo-pixels, and two 516 pixel analog CCD shift registers. Upon triggering the transfer gates (ϕX_A,ϕX_B), the odd-numbered pixels shift in parallel into the B shift register and the even numbered pixels shift into the A shift register. The data are then shifted out of the shift registers in serial through two charge-sensitive pre-amps at half the basic clock rate. These two video data channels are combined off chip to form the valid video data. The 13 x 13 μm contiguous photo-pixels are shown in Figure 3.5.

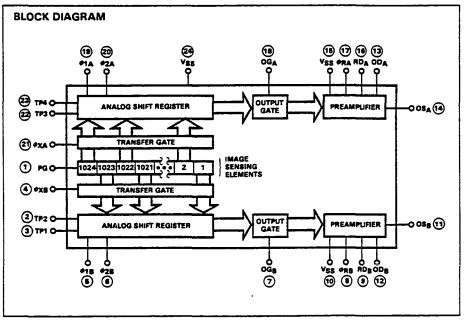

Fig. 3.4. Block diagram of the Fairchild 131 linear CCD (courtesy of Fairchild Co.).

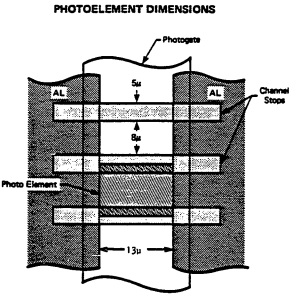

Fig. 3.5. 13x13 µm pixels (photo-element) of the CCD.

The CCD board (built by the Naval Training Equipment Center) derives the eight correctly phase timing signals from an off-board oscillator. It contains counters for operating the CCD in free run mode and a series of special purpose TTL-to-MOS drivers for powering the internal shift registers. (Unlike more current devices, the model 131 derives all its power from the input clocks.) Most of the circuitry contained on the CCD board is contained on the CCD chip in the newer generation CCDs.

In strobed mode the data transfer gates are triggered first by the computer to clear the photo-pixels and then are triggered again after the requested integration time. After the second data transfer trigger, the data leaving the video combining/amplifying circuit are digitized. In practice, because the array is left unread between exposures, it saturates. Therefore it becomes necessary to strobe the transfer gates approximately six times (the current software does this nine times for safety) before the data in the shift registers becomes valid (free of stray charge).

In free-running mode, counters on the CCD board are enabled. After every 1036 clock cycles, the data transfer gates are triggered, dumping the data into the shift registers and out through the pre-amps. The free-run mode integration time is thus 1036 multiplied by the basic clock period. Free-run/strobe mode is selected by a switch on the interface electronics box.

The interface electronics box contains a circuit card with the video amp circuit, two reed relays and logic to control the direction of

the motorized stage, the op-amp circuit for the temperature sensor, and the external clock supplied to both computer and CCD board. The box also contains a 15 volt commercial power supply that is regulated in the box down to ±12, +8, and +5 volts, all of which are required and supplied to the CCD board. The video combining/amplifier circuit uses a 4066 CMOS switch to combine the odd/even pixel flow. Each video data line from the CCD charge sensitive preamps is passed through a LF-356 op amp for impedance isolation and to correct for DC offset and gain between channels. One of the major problems with the amplifying circuitry on the NTEC board is that there is no correction for the temperature dependent offset and gain. Except for devices that are optimized for extremely high speed operation, current CCDs pass all the data through the same charge sensitive pre-amp to avoid this problem. These signals are then combined by the 4066 switch, amplified by a third LF-356 op-amp, and sent to the A-to-D converter over coaxial cable terminated into 200 ohms. A National LH-002 current amplifying instrumentation op-amp was originally piggy-backed on the final LF-356 op-amp to provide the current drive necessary to terminate the coaxial cable into 50 ohms, but under certain conditions this set up oscillations from the transfer gate that leaked through the closed end of the 4066 switch. A reasonable solution was to terminate with 200 ohms, which can be handled by the LF-356 op-amp alone. There is no apparent degradation of the data by reflections from the improperly terminated cable.

The video sync circuit synchronizes the data transfer strobe from the LSI-11 to the external clock. The derived data transfer signal

is then sent to the CCD board, and used to enable a counter that blanks the digitized strobe line sent back to the computer until after data from the first eight nonvalid photo-pixels have passed. This insures that the computer sees data from pixel nine as the first data element to be digitized. Without the addition of the counter we were unable to sync to the first pixel without a ±1 pixel error, which had to be corrected in software. This error becomes important because we add 16 dark frames together and 16 data frames together and subtract the two, increasing the dynamic range of the CCD by four. With a ±1 pixel error, the fixed pattern noise would not subtract out and an additional noise term would enter. (This was the other major problem with the NTEC board.)

Figure 3.6 shows a circuit diagram of the video sync interface circuit and Figure 3.7 the two-channel video combining/amplifying circuit.

Cooling and Power Monitoring

The CCD is cooled on the backside by a thermoelectric cooler that is sandwiched between the array (cold side toward the array) and a copper heat pipe. The other end of the heat pipe is placed in an ice bath that acts as a thermal reservoir for the hot side of the thermoelectric cooler. The array temperature is monitored by measuring the forward bias drop of a small diode placed in contact with the backside of the array. A linear fit to the voltage drop vs temperature data is used to calculate the array temperature (Figure 3.8). The wedge--CCD array--thermoelectric cooler assembly is shown in Figure 3.9.

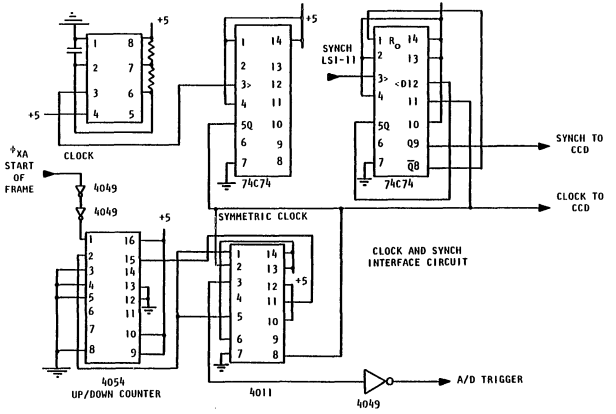

Fig. 3.6. Diagram of the LSI-11/CCD clock interface circuit.

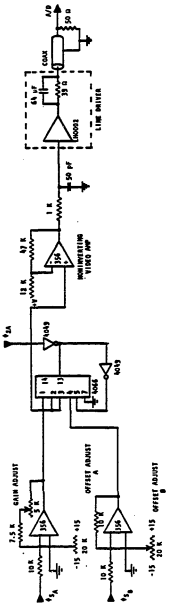

Fig. 3.7. Video channel combining/amplifying circuit.

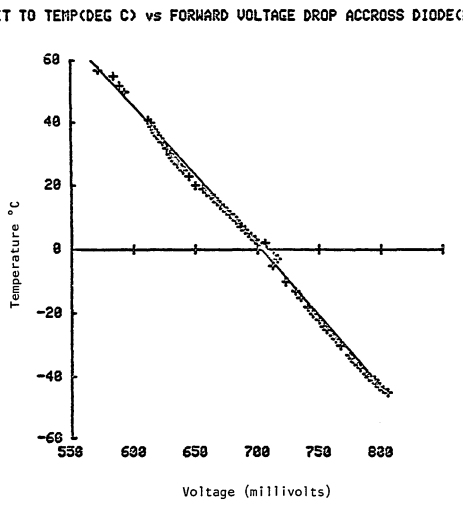

Fig. 3.8. Linear fit to data for temperature (°C) vs voltage drop across the temperature measuring diode.

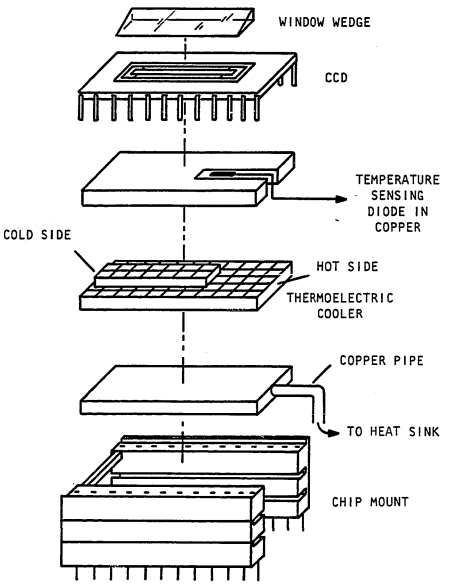

Fig. 3.9. CCD, optical wedge, and thermoelectric cooler assembly.

It is possible to reduce the operating temperature of the array from approximately 36°C to 12°C before condensation on the CCD window becomes a problem. A reduction in operating temperature of 24°C yields an improvement in signal to noise of about 8. In addition, cooling the detector below 12°C introduces strain on the CCD chip and mount, which results in a bad video data line. Thus operating the array at significantly lower temperatures would require a thermally compliant mount that would enable the array to be placed in a nitrogen or vacuum environment.

The laser power is monitored by a photodiode/operational amplifier pair. About 4% of the light from the argon laser is split off by an uncoated flat and falls on the photodiode. The signal from the transimpedance op amp is calibrated against the laser power after it has been spatially filtered and collimated. A four-parameter polynomial fit to the data (Figure 3.10) is used to calculate the laser power.

Software

Software for running the experiment is written in FORTRAN with Macro-11 (assembly language) callable subroutines for operating the hardware such as the CCD array, stage, etc. With the exception of the Fast Fourier Transfer Routines (Bergland and Dolan, 1979), all of the software is original. Because the memory space of the LSI-11 (32K, 16 bit words, with the upper 3K reserved for the BIOS and overlay handler) is too small to hold the entire program, the program is broken down into a root segment and three overlay segments sharing the same memory space.

The write protect and cursor addressable position features of the Soroc IQ-120 terminal are used to display a fixed menu, while current

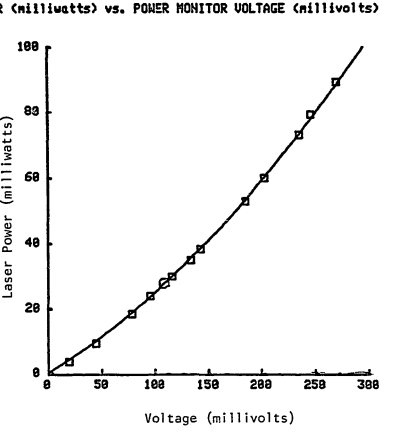

Fig. 3.10. Power vs voltage from the power monitoring photo-diode/ operational amplifier pair, and polynomial fit to the data.

system parameters and data are displayed in the unprotected portion of the field. The keyboard is interrupt driven and branches to that portion of the program called by the operator from the menu.

Data may be stored either as single data frames cataloged and retrievable from the library menu, or as mass storage in a separate file. The second option is used for large data sets created by stepping the stage containing the sample under study. In the case of single data frames, a title and run number are entered and cataloged, and the date, operating temperature, speckle contrast, integration time, laser power, integrated irradiance, and A to D gain are stored as part of the record.

CCD Window

A problem common to many optical measurements in coherent light is multiple reflections from the detector window. The contrast values measured with our CCD were reduced from their true values by these multiple reflections. This was observed when measuring a fully developed speckle pattern of known, unity, contrast.

This problem was corrected by index matching a wedge to the CCD window using mineral oil. Another solution would be to use a backside illuminated, thinned CCD.

Noise, Subtraction, and Error

The limiting sources of noise with the described instrumentation are dark current noise, fixed pattern noise, nonuniform pixel responsivity, and noise introduced by the charge-sensitive and video pre-amps. Fixed pattern noise (actually fixed nonuniformities in the dark current) is generally separated from the random dark current background. Other

sources of noise such as trapping noise or electrical input noise are generally measured in the tens and hundreds of electrons (Barbe and Campana, 1977) and are of little significance for our instrumentation.

The nonuniform pixel responsivity was measured by illuminating the CCD with spatially uniform light generated by an extended white light source at a long distance from the array and placing a 450 nm to 550 nm bandpass filter in front of the array. We tested both of our model 131 chips and used the better chip, which had (less than) 4% peak-to-peak variation in the responsivity when the temperature was lowered below 18°C.

Figure 3.11 shows three exposures taken from the CCD, digitized, and displayed on an oscilloscope. The integration time was 500 ms and the array was uncooled and operating at 34°C. The first exposure is a background frame taken with the laser off. The fixed pattern noise is the negative sloping of the data plus the popcorn noise of various pixels above the well defined data line. The second frame is an exposure of a speckle pattern where the signal is approximately equal in magnitude to the fixed pattern noise. The third frame shows the subtraction of the first exposure from the second, which is performed in memory after digitizing the first two frames. By subtracting a dark frame from a data frame it is possible to null the fixed pattern noise.

A second technique to reduce noise is to signal average the speckle pattern. If the array operates at 18°C (the usual operating temperature), the maximum RMS signal-to-noise ratio (the dynamic range of the CCD) is 8 bits with the above subtraction technique. By averaging

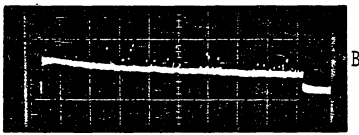

(a)

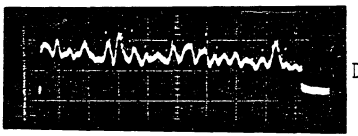

(b)

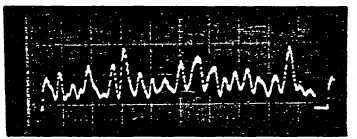

(c)

Fig. 3.11. Digitized speckle data.

(a) Background frame, laser off.
(b) Data frame, laser on.
(c) Background frame subtracted from data frame.

over 16 frames, the signal-to-noise ratio was increased to 12 bits, which is the accuracy of the A to D converter.

To calculate the effect of noise on the speckle contrast, we consider the signal from the jth pixel as the sum of three terms:

I_j, the irradiance of the incident speckle pattern;

F_j, the fixed pattern noise; and

N_j, all other noise sources.

If we subtract a dark frame from a data frame as above, the signal from the jth pixel becomes

$$S_j = (I^1{}_j + F^1{}_j + N^1{}_j) - (F^2{}_j + N^2{}_j) \quad , \tag{3.3}$$

where the superscripts 1 and 2 represent the data and dark frames respectively. The expected value of the average signal is then the expected value of the average irradiance because the noise terms have equal (and presumably zero although this is not necessary) means. A hat over an expression means a measured quantity. Therefore the average signal is defined as

$$\begin{aligned} \langle \hat{S} \rangle &= \left\langle \frac{1}{M} \sum_{j=1}^{M} S_j \right\rangle \\ &= \left\langle \frac{1}{M} \left[\sum_{j=1}^{M} I^1{}_j + \sum_{j=1}^{M} (F^1{}_j - F^2{}_j) + \sum_{j=1}^{M} (N^1{}_j - N^2{}_j) \right] \right\rangle \\ &= \langle I \rangle = I \end{aligned} \tag{3.4}$$

where M is the number of pixels. The expected value of the standard deviation is not zero, but contains a bias due to the finite standard

standard deviation of the noise, that is,

$$\sigma_s^2 = \left\langle \left(\frac{1}{M-1}\right) \sum_j (S-\langle\hat{S}\rangle)^2 \right\rangle$$

$$= \left\langle \left(\frac{1}{M-1}\right) \sum_{j=1}^{M} (I_j-\langle I\rangle)^2 + \left(\frac{1}{M-1}\right) \sum_{j=1}^{M} (N_j{}^{1^2}+N_j{}^{2^2}) \right\rangle$$

$$= \sigma_I^2 + \sigma_n^2 \qquad (3.5)$$

In the standard deviation of the noise there is a term proportional to $(N_j{}^1)^2 + (N_j{}^2)^2$ that is not necessarily zero because the noise from each pixel is squared and then added. This non-zero standard deviation of the noise may be considered to be a bias term added to the standard deviation of the irradiance. For a completely developed speckle pattern with a theoretical contrast of one, the measured contrast can be expressed as

$$\langle\hat{C}\rangle = \frac{\sigma_s}{\langle\hat{S}\rangle} = \frac{\sqrt{\sigma_I^2 + \sigma_n^2}}{\langle I\rangle}$$

$$\approx \frac{\sigma_I}{\langle I\rangle} + \frac{\sigma_n^2}{2\sigma_I\langle I\rangle} = C + \frac{\sigma_n^2}{2\langle S\rangle^2} \qquad (3.6)$$

Thus the non-zero standard deviation of the noise adds a bias term to the measured value of the contrast equal to the expected value of the noise variance divided by twice the average signal.

To measure the expected noise variance, the shutter was turned off and we performed 500 measurements of one scan length (1024 pixels) in a normal fashion. A typical noise frame is shown in Figure 3.12. The

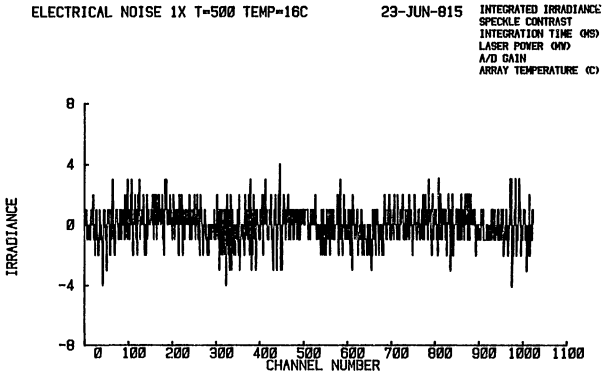

Fig. 3.12. Noise from a typical contrast measurement.

noise variance was found to be approximatly 3 bits, and the average noise was 0. For a typical contrast measurement with an average signal of about 32 bits, substitution into Eq. (3.6) shows a bias in the measured contrast of about 0.5%.

The conclusion is that the noise terms from the CCD do not bias the measured value of the contrast. By subtracting the dark noise from the data and averaging over 16 data frames, the average noise from the array is essentially nulled. The effect of the non-zero noise standard deviation is shown to be less than 1% for a typical measurement.

CHAPTER 4

MEASUREMENTS OF A FULLY DEVELOPED SPECKLE PATTERN

The first order probability density of the irradiance and power spectra of a fully developed speckle pattern, and the modulation transfer function (MTF) of a linear CCD array were used in Chapter 2 to calculate the contrast measured by a CCD as a function of speckle and pixel size, and to calculate the first order statistics (the probability density) of the contrast. This chapter is devoted to the experimental verification of the theory developed in Chapter 2.

The contrast of fully developed speckle measured by a CCD detector array is less than its theoretical value of 1 primarily because of spatial integration over the finite size of the detector pixels, and is only slightly degraded due to charge transfer inefficiency for $\lambda \leqslant 600$ nm. Ultimately we are interested in measuring partially developed speckle patterns of reduced contrast. Because the power spectra of these patterns is unknown, it is not possible to correct for the effects of the detector MTF on the measured contrast. Thus we want the contrast degradation to be as small as possible. This explains our interest in the contrast as a function of the sampling parameter γ (Chapter 2), which for a fixed pixel size is a function of the effective F# of the imaging lens.

The number of pixels in any one CCD frame limits the number of speckles intercepted by the detector array. This limited number of speckles (limited sample space) is used to compute the contrast. The

probability density of the contrast can be used to determine the statistical significance of a contrast measurement with a finite number of speckles present. As shown in Chapters 2 and 3, the limiting noise of this experiment would not be instrumental error if the data from a single CCD frame was used, but is uncertainty due to the small number of statistically independent data points (speckles).

A fully developed speckle pattern was created by a beaded screen in reflection and a ground glass plate in transmission. The agreement between theory and experiment is good for both the contrast as a function of the sampling parameter γ, and for the probability density of contrast.

Rough Surfaces

The theory in Chapter 2 was based on a fully developed speckle pattern because the statistics are well known and exist in closed form, and because it is the most severe (or random) speckle pattern obtainable and so represents a worst case analysis. One of the assumptions used to form the statistics of a fully developed speckle pattern is that the phase distribution of the electric fields at the image plane are uniform over modulo 2π. This is the rough surface approximation where the surface roughness is assumed to be larger than λ, so the phase excursions $(2\pi OPD/\lambda)$ of the different phasors will be many times 2π. Thus the surface used to create these speckle patterns must be consistent with the approximations used to derive the theory.

Two different surfaces were used to verify the theory of Chapter 2; a ground glass plate used in transmission, and a beaded screen used in reflection. To make sure the rough surface approximation was met,

both surfaces were tested with a stylus type surface profilometer. The output of this instrument is a trace on a strip chart recorder which is proportional to the surface height of the sample. A sample trace across 4 mm of the beaded screen is shown in Figure 4.1. From several traces like these we concluded that the RMS roughness of the ground glass is approximately 0.8 μm with peak to peak variations of about 3 μm. The RMS roughness of the beaded screen is between 3 and 5 μm, with peak to peak variations of approximately 12 μm. While the beaded screen is considerably rougher than the ground glass plate, both surfaces have height variations that satisfy the rough surface approximation.

Experimental Configuration

The experimental configuration used for measuring the properties of a fully developed speckle pattern is shown in Figure 4.2. The major experimental concerns were the $\cos^4\theta$ fall off in irradiance at the edge of the field of the imaging lens, and the Gaussian irradiance profile due to the laser source. The $\cos^4\theta$ fall off was minimized by working with a long back focal distance from the imaging lens to reduce θ. For the given experimental configuration, the chief ray angle was 0.15°, and $\cos^4\theta$=1.000. The effect of the non-uniform irradiance profile was reduced by overfilling the collimating lens so that the irradiance across that section of the ground glass imaged onto the CCD array was uniform. The electric field amplitude transverse to the direction of propagation, E(r), is given by (Siegman, 1971)

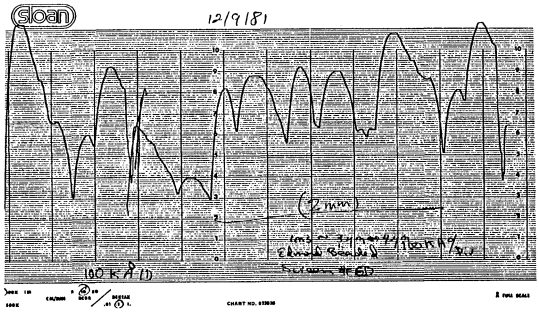

Fig. 4.1. Example of a Tallystep trace across a beaded screen, 0.4 mm/horizontal division and 10 μm/vertical division.

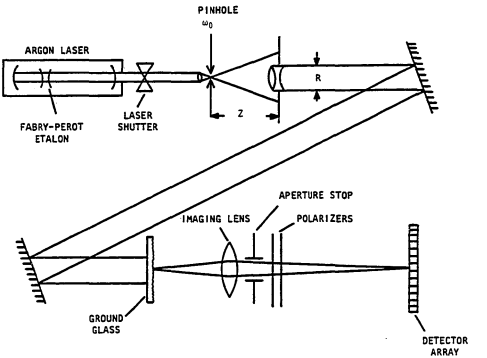

Fig. 4.2. Experimental configuration for measuring speckle contrast of a fully developed speckle pattern.

$$E(r) = \left(\frac{2}{\pi}\right)^{\frac{1}{2}} \frac{1}{w(z)} e^{-r^2/w(z)} \tag{4.1}$$

where w(z) is the beam waist parameter, which can be approximated in the far field as

$$w(z) \approx \frac{\lambda z}{\pi w_o^2} \tag{4.2}$$

z is the distance from the minimum waist size (spot size), w_o, to the plane of observation. From Figure 4.2 with w_o=25 μm, z=1270 mm, λ=.5 μm, the irradiance is reduced from the center of the array (r=0), to the edge of the array (r=2.45 mm) by $|E(r)/E(o)|^2$=0.16. The object height is half the CCD array height (6.66 mm) divided by the image-to-object transverse magnification (2.7).

A second polarizer was placed after the first to insure that the field illuminating the CCD was truly plane polarized. We noticed about a 1% increase in the contrast by using a second polarizer, but no additional increase in contrast when a third polarizer was added. This indicated that the speckle was not completely plane polarized after using a single polarizer. The aperture stop was a piece of aluminum with various diameter holes drilled in it, except for the 1 mm and 2 mm aperture stops which were made by poking a hole through sheet brass with a sewing needle.

The image plane was found by placing a mask in the object plane and focusing (by eye) for maximum sharpness. As the longitudinal depth of field of the speckle is approximately $(2\lambda F\#)^2$, and F# is always greater than 60 for sampling reasons, the correct focal position is not

critical. Collumnation of the spatially filtered beam was checked with a shear plate. While small amounts of defocus in the incident beam should not effect the contrast, collimation was introduced in the experiment for convenience. A Fabry-Perot etalon was placed in the laser cavity to insure single mode operation. The Fabry-Perot was placed in the laser cavity to insure that the small discrepancy we see between theory and measurement (Figure 4.3) is not due to multi-mode oscillation in the laser cavity. A paper tunnel covered the path from the ground glass to the detector array to block out stray light and the laser shutter was placed close to the laser exit aperture for the same reason.

Contrast as a Function of Aperture

The contrast of a fully developed detector array is less than its theoretical value (1) because of spatial averaging by the finite size of the array pixels, and image smear due to charge transfer inefficiency. The effect of photo-electron diffusion for $\lambda \lesssim 600$ nm is negligible (Barbe and Compana, 1977). Since the effect of this process is most easily expressed in terms of the MTF each process gives rise to, and also because the cumulative effect due to both is the multiplication of the individual MTFs, the natural domain for calculating the effects of the array on the measurement is in frequency space. In Chapter 2 an expression for the contrast was developed in terms of sampling parameter γ, where

$$\gamma = \frac{\text{maximum spatial frequency of the speckle pattern}}{2 \text{ x the Nyquist sampling rate of the CCD}}$$

$$= P/\lambda F\# \qquad (4.3)$$

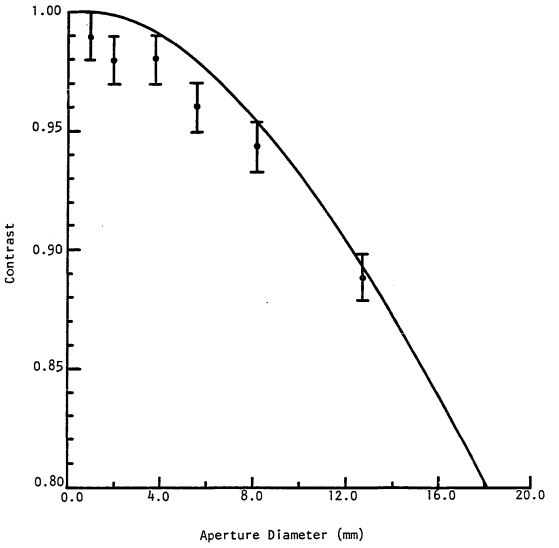

Fig. 4.3. Contrast as a function of aperture diameter. The Nyquist frequency is reached at 17.2 mm.

P is the pixel width, and F# the effective F number of the imaging lens in image space. For the fixed pixel width, wavelength, and imaging geometry shown in Fig. 4.2, γ is determined by the diameter of the imaging lens, a, as

$$\gamma = 0.029\ a \tag{4.4}$$

where a is in mm.

As the aperture increases, the maximum spatial frequency of the speckle pattern increases. The scale of the power spectra is changing so that its form (Fig. 1.3) does not change, but it is being stretched along the frequency axis. Thus γ is a measure of that portion of the bandwidth of the CCD that the speckle pattern occupies in frequency space. As γ increases (a increases), the CCD is called on to measure higher spatial frequencies. Since the response of the CCD decreases for increasing spatial frequency, the amplitude of the high frequency components becomes increasingly smaller and the contrast is reduced.

An alternative, more intuitive way of viewing the contrast reduction with increasing aperture, is to look at the problem in the spatial domain. The speckle size is $1.22\lambda F\#$. As the aperture becomes larger the speckles become smaller and the sampled pattern becomes less like the image incident on the array due to the discrete and finite nature of the pixels of width p. This averaging reduces the contrast.

The contrast was measured for 6 different aperture stops ranging from 1 mm to 12.7 mm, which is almost out to the Nyquist sampling rate at 17.2 mm. For each aperture stop, the data from 40 frames was treated

as a single statistical record yielding a minimum number of speckles (for a = 1 mm) of approximatley 1,200. The results of these measurements, along with the theoretical curve for the contrast (Fig. 2.6) which has been rescaled as a function of aperture size, is shown in Figure 4.3. The ±1% error bars were derived from the repeatability of the measurement.

Probability Density of the Contrast

Early experiments with our experimental apparatus showed that, for a fully developed speckle pattern, there was a large spread in the contrast calculated from the data in a single CCD frame. The reason for this is the statistically small sample space one is forced to work with in order to correctly sample the speckle pattern. We were able to solve this problem because the surface under test is stationary, and we are under no time constraints in performing the measurement.

A computer controlled remote stage was built to step the sample so that different portions of the surface could be imaged onto the detector array. After the requisite number of frames are recorded, the contrast is computed treating all the data frames as a single data record. (This is not the same as taking many frames of data and averaging the contrast from each frame.) Thus we have avoided the problem of the statistically small sample space by taking many frames of data.

However, we remained interested in the significance of the contrast as determined by a single frame of data for the following reason. Over the last several years there has been much speculation that speckle measurements might be useful as an industrial tool for testing surface roughness. In an industrial environment, such as along an assembly line,

testing a piece must be accomplished quickly, and only once. The confidence level one has in using a limited data set to measure surface roughness will determine whether an automated decision making process can be used.

In Chapter 2, a Monte-Carlo simulation of the contrast as a function of the number of speckles across the detector array was performed. The results of this model are shown in Fig. 2.5. For small number of speckles, the peak contrast moves to smaller values than one, and the standard deviation of the contrast increases. As more and more speckles are added (the aperture of the imaging lens is widened) the standard deviation of the contrast becomes smaller, and the peak value moves towards one.

520 frames of data (0.5 Megapixels) were taken with a 2 mm aperture pinhole of the speckle created from a beaded screen. From Eqs. (4.4) and (2.20), the approximate number of speckles per frame is 48. A histogram of the frame by frame contrast is plotted in Fig. 4.4 along with the Monte-Carlo calculation for 50 speckles per frame calculated in Chapter 2. The measured average contrast and standard deviation were 0.966 and 0.131 respectively. The predicted average contrast and standard deviation were 0.981 and 0.127 respectively. Figure 4.4 clearly shows the bias towards lower values of the contrast with a long tail reaching out towards large values of C.

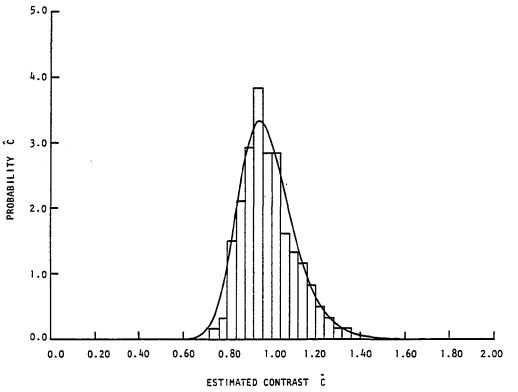

Fig. 4.4. Probability density of the contrast.

Solid line curve is the Monte-Carlo simulation for m=50 (Chapter 2). Histogram is compiled from measurements where m=48.

CHAPTER 5

SPECKLE CONTRAST REDUCTION FROM FLUORESCENT SCREENS

At the request of the Naval Training Equipment Center, our first attempts to reduce the speckle in laser projection systems was to coat the screen with either a dye, phosphor, or paint. The absorption of the laser illumination and fluorescence by the material decreases the coherence length of the light returned to the viewer's eye, thus reducing the speckle contrast. The primary advantage of this method is that any previously built laser projection system could be retro-fit with a coated screen without hardware modification. The disadvantages are that coated screens have inherently less gain, and there would be difficulty in finding a material that could be used with a multi-color display. (Pinhow, Van Uitert, and Feldman, 1971, have made several interesting suggestions for building a multi-color display using a single wavelength laser. Their technique would require building a screen with a complicated internal structure and substantial hardware modifications in the projection system.)

Materials and Coating Methods

We tested 2 commercially available dyes in film form (from the 3M Co.), several inorganic phosphors suggested in a paper by Van Uitert, Pinnow, and Williams (1971) and by the staff at GTE Precision Materials, and fluorescent spray paints. Our first attempts to coat the screen with inorganic phosphors was to spray an adhesive onto the screen and then

lightly dust the surface with phosphor. Samples produced this way were unevenly coated, and produced results that were not consistent on a sample to sample basis, or even across the same sample. GTE (who, along with The Harshaw Chemical Co., supplied the phosphors) suggested we built a settling chamber and use a dispersing agent (PS-6) to control the amount of phosphor used, and to get an even coating. They suggested an optimum coating surface density of approximately 8 mg/cm^2.

The settling chamber we built was a 6 x 6 inch section of a fish aquarium that had been partitioned off and raised on blocks. The procedure for coating a sample was (following GTE's instructions)

1 - place 3 liters of distilled water in the chamber along with slides

2 - add 34 ml of 1% barium acetate solution

3 - disperse 1.86 g of phosphor in 34 ml of PS-6 solution and add 100 ml of distilled water

4 - shake solution and pour into dispersing funnel

5 - rinse flask with 25 ml of distilled water and pour into dispersing funnel

6 - wait 2 hours for the solution to settle, and the slides to become coated

7 - slowly decant the liquid by siphoning (One has to be careful to do this slowly, or the phosphor coating will be disturbed and ruined)

8 - allow the slides to dry in air for at least 24 hours.

1.86 g of phosphor yields the recommended 8 mg/cm^2 surface density.

We also tried testing two organic dyes, Rhodamine 6G (used often in Argon pumped dye lasers) and Ethelyne Glycol (automobile anti-freeze), that fluoresced when stimulated with visible light. These dyes were combined with an acrylic binder to get these materials to dry and stick to a screen. However, we were unable to combine a large enough quantity of the dye with the acrylic to get both significant speckle reduction, and have the dyes dry and stay on the screen.

Two types of films imbedded with dyes (3M Co. #3484 and #3485) were then tested, and two different fluorescent spray paints (Zynolyte #1403 and #1402) were also tested for speckle reduction. The films come with their own backing material and are uniformly thick. We attempted to keep the surface layer thickness constant when spray painting a screen sample by making six passes over the surface with the spray nozzle approximately 2 feet (one arms length) from the surface.

Screen Gain

It is somewhat misleading to compare the light intensity of an uncoated beaded screen sample with coated samples because the coating covers the beads which provide the screen gain. The coated surface acts more like a Lambertian surface, as opposed to the beaded surface in which the screen radiance is a function of angle. For the film samples, the backing on the films is flat and these films also act Lambertian.

A possible solution to decrease the speckle and yet retain the gain properties of a beaded screen is to coat a flat surface with the desired phosphor, paint, or dye, and then try attaching the beads to the

surface so that the diffraction due to the beads will not be impeded by the coating. We attempted to attach glass micro-balloons to a coated surface by spraying an adhesive onto the surface, and then dusting the surface with the micro-balloons. We found however, that the density of beads that could be achieved without clumping was very low, and so again there were problems in achieving even coatings.

Thus, while a great deal of time was spent performing the work in this chapter, the work does not optimize the speckle reduction and gain characteristics of coated screens. A comparison of the percentage of light returned by each material is useful for comparing the efficiency of each material within its group, or for comparing how a particular material applied exactly as we have done, will reduce the irradiance over the irradiance returned by an uncoated, ordinary, beaded front projection screen. (An Edmund Scientific beaded screen was used as the standard beaded screen.) It was felt that an in depth study of all of the above materials and coating techniques (or new materials and coating methods) was beyond the scope of this dissertation.

A second problem is that the spectral response of the array is different from the spectral response of the human eye for $\lambda \geqslant 550$ nm. Since the irradiance is the integral of the spectral response of the detector multiplied by the source spectrum, the contrast perceived by a viewer for a multi-color display will be different than what is measured by a CCD detector. We did explore the possibility of purchasing a filter so that the filter-CCD array combination had the same response as the human eye, but found the cost prohibitive.

Experimental Measurements

The configuration used to test the various screen surfaces is shown in Figure 5.1. A cylinder lens was used to illuminate a narrow bar on the sample, rather than a circular area, to increase the signal-to-noise ratio. In all cases, except for the 3M films, the surface was oriented so that the specular angle of reflection was pointed towards the detector array, although the results did not seem to vary as the sample was tilted a few degrees in either direction. Because there was a specular reflection off of a plastic coating covering the dyes in the 3M films, these were oriented so that the specular reflection was not pointed into the CCD. In addition, when illuminated with enough laser light to get a reasonable signal-to-noise from these films, they would heat up and the speckle would appear to "breathe" (change its structure slowly), until they reached an equilibrium state. To avoid this problem a 20 second wait state was inserted in the software after moving the sample carrying stage, but before taking data. The percentage of irradiance was calculated as the difference between the average irradiance of the sampled surface (the area underneath the speckle pattern), divided by the average irradiance from an uncoated beaded screen. 40 frames of data were used to calculate the speckle as a single data set, and each data set was repeated several times.

The results of measuring the speckle contrast and percent reduction in irradiance are shown in Table 5.1, and sample data frames are shown for a dye, spray paint, and phosphor in Figure 5.2 a-c. Both as measured by the CCD, and as viewed through a pinhole, the maximum speckle reduction was due to the Rhodamine 6G. The problem was that there is

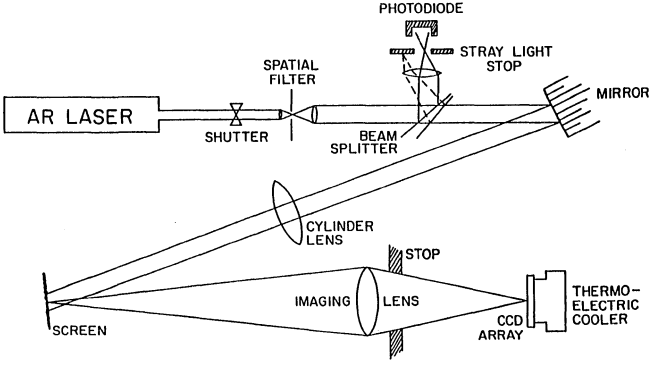

Fig. 5.1. Experimental configuration for measuring the contrast of beaded screens.

Table 5.1. The contrast measured from coated screens for the various materials tested.

SURFACE TYPE	CONTRAST	% REDUCTION IN IRRADIANCE
$Y_{2.94}Ce_{0.6}Al_5O_{12}$ (HARSHAW)	0.78	33
$Y_{2.88}Ce_{12}Al_5O_{12}$ (HARSHAW)	0.71	32
P-24 #149 (SYLVANIA)	0.62	36
FX-501SC #122 (SYLVANIA)	0.78	32
CGY-505 #1230 GREEN (SYLVANIA)	0.72	34
YELLOW FLUORESCENT PAINT	0.59	36
GREEN FLUORESCENT PAINT	0.63	37
RHODAMINE 6G FILM (SCOTCH #3484)	0.13	79
YELLOW FILM (SCOTCH #3485)	0.39	77

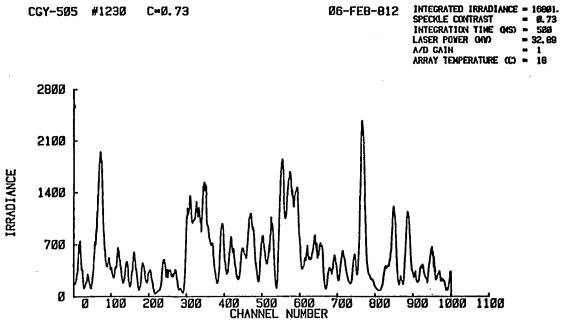

(a)

Fig. 5.2. Sample data, speckle reduction from coated screens.

(a) GTE CGY-505 #1230 phosphor.

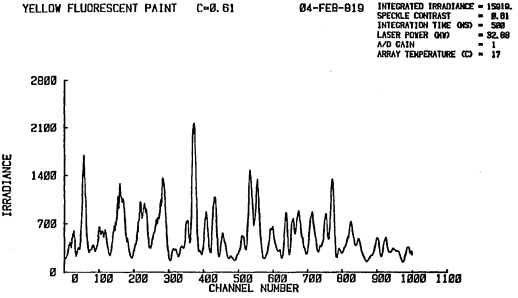

(b)

Fig. 5.2.--Continued

(b) Yellow fluorescent paint (Zynolyte).

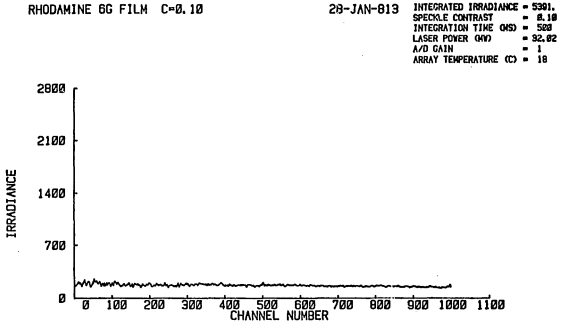

(c)

Fig. 5.2.--Continued

(c) Scotch film #3484.

also a very large reduction (again, as viewed by an observer, and measured by the instrumentation) in the irradiance from the sample. A best case can be made for the yellow fluorescent spray paint. There is good speckle reduction, it is easy to apply to a screen, and there is good light efficiency.

CHAPTER 6

SPECKLE MULTIPLEXING FOR CONTRAST REDUCTION

Speckle reduction techniques for projection or display systems fall into the areas of reducing the coherence of illumination, or optical multiplexing techniques where more than one uncorrelated (or partially correlated) speckle pattern is incoherently summed during the integration period of the detector. In Chapter 5 we discussed changing the temporal coherence of light reflected from the screens by coating the screen surfaces. In this chapter we discuss multiplexing techniques for incoherently adding several speckle patterns together to form a speckle pattern of reduced contrast. For M uncorrelated speckle patterns with identical statistics and average irradiances, the contrast is reduced by $(1/M)^{\frac{1}{2}}$ (Goodman, 1976). The more complicated problem of partially correlated speckle patterns is handled by orthogonalizing the partially correlated set and using the magnitude of this new, uncorrelated set to compute the contrast.

A common fallacy is to believe that the motion of the laser spot across the screen surface should, by itself, reduce the speckle noise. For linearly scanned displays, the amount of speckle reduction depends on the point spread function (PSF) in the object plane. The number of uncorrelated speckle patterns, M, from any position on the screen is the number of laser spots that will fit within the PSF of the observers eye.

If the laser spot is larger (or approximately equal) to the PSF, only one speckle pattern appears from any point on the screen, and the contrast is not reduced. However, if several laser spot diameters fit within the viewers PSF, these speckle patterns will be integrated by the slower time response of the eye. This integrated speckle pattern, of lower contrast, will appear from a single position on the screen. Thus, a simple technique to reduce laser speckle is to reduce the spot size of the projection beam so that it is many times smaller than the viewers PSF. In some systems this may be practical, but in others the increase in the tolerances and aberration correction of the projection optics, and the increase in the bandwidth of the scanning system (which is proportional to the increased number of resolvable points) makes this option impractical.

In this chapter we discuss changing the angle of illumination of the projection beam at the same position on the screen to create a diversity of speckle patterns. This technique uses a large laser spot, and can significantly reduce the contrast of a laser display. We also discuss speckle reduction by polarization diversity. The reduction in contrast from two orthogonal speckle patterns is smaller than from scanning techniques because the maximum number of uncorrelated speckle patterns is only 2.

Speckle Diversity by Polarization

The addition of orthogonally polarized speckle patterns must be an incoherent addition. If the speckle patterns produced by orthogonal polarizations from the same scattering area on a screen are uncorrelated

(or partially correlated), the integrated speckle pattern will have a lower contrast than the individual speckle patterns. However, if both component speckle patterns are identical (or very similar), no (or little) speckle reduction will occur. If uncorrelated or partially correlated speckle patterns do occur, these patterns may be populated by placing a quarter wave plate into the (usually) linearly polarized Argon laser, or by internal de-polarization of the screen itself.

Early measurements made on various screen samples showed that if a polarizer was removed from the measurement configuration the contrast was reduced. We speculated at that time that this reduction in contrast was due to de-polarization of the reflected light by the screen. With this in mind, we returned to study how the speckle pattern of ground glass and a beaded screen change with changing incident polarization.

By simply looking through a polarizer at the reflected or transmitted light from a beaded screen or ground glass plate, it was apparent that the screen depolarized plane polarized light from an argon laser with almost equal irradiance at all angles of polarization, but that the ground glass did not.

A half wave plate was placed in the incident beam and rotated to change the angle of polarization of light transmitted by a ground glass plate. Figure 6.1a,b,c shows the almost identical speckle patterns created at polarization vector angles of 0°, 90°, and 135°. Because there is almost perfect correlation between these patterns, little or no contrast reduction would be expected if the ground glass were illuminated with both polarizations. Figure 6.2 shows the effect on the speckle pattern and the contrast of placing a quarter wave in the incident beam. As

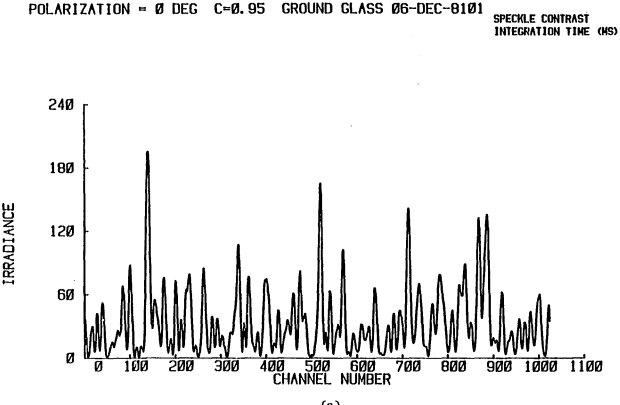

(a)

Fig. 6.1. Polarized speckle from a ground glass screen.

(a) Polarization angle = 0°.

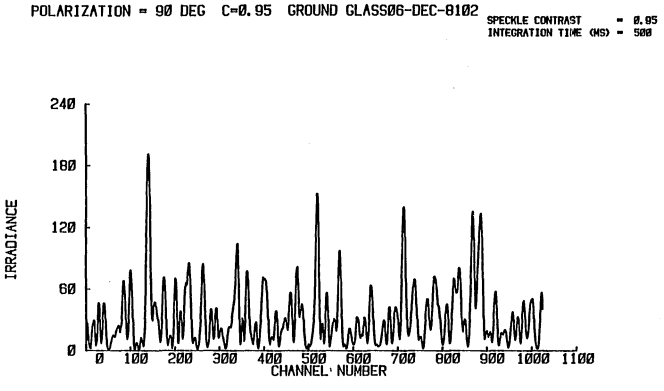

(b)

Fig. 6.1.--Continued

(b) Polarization angle = 90°.

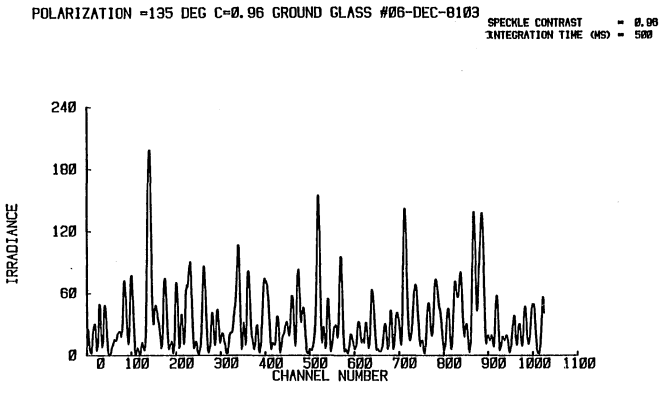

(c)

Fig. 6.1.--Continued

(c) Polarization angle = 135°.

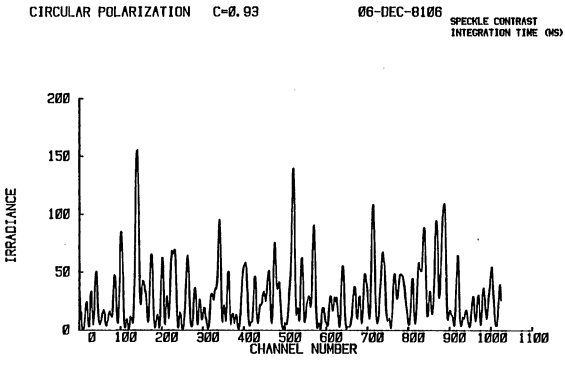

Fig. 6.2. Unpolarized speckle produced with a quarter wave plate in the incident beam.

expected, there is little change in the speckle pattern, and a very small reduction in contrast.

However, for a beaded screen where different speckle patterns were obtained at different polarization angles (Fig. 6.3), significant contrast reduction should occur when two orthogonal polarization components are present. Since the screen itself depolarizes the reflected light, it was interesting to introduce a quarter wave plate to see the effects of complete polarization diversity. Figure 6.4 shows the same speckle pattern as in Fig. 6.3 except that the polarizer between the screen and the detector was removed. The speckle in Fig. 6.5 was measured identically to that of Fig. 6.4 except that a quarter wave plate was inserted into the beam to equalize the incident irradiance at orthogonal polarizations. There is a large drop in the contrast and a substantial change in the structure between the speckle patterns with and without a polarizer present (Figs. 6.3 and 6.4). However, there is only a small change in structure and contrast between unpolarized speckle patterns produced with and without a quarter wave plate present (Figs. 6.4 and 6.5). This indicates that depolarization by the beaded screen is almost complete. Since the resultant contrast from an ordinary beaded screen is .86, the speckle at orthogonal polarizations is not completely decoupled. Table 6.1 is a compendium of the contrast from the various uncoated screens we studied. The contrast varied from 0.93 for a ground glass surface in transmission to 0.79 for a high gain beaded screen (3M #7915).

To summarize this section, a 10% contrast reduction can be gained by projection on screens rather than through ground glass due to the

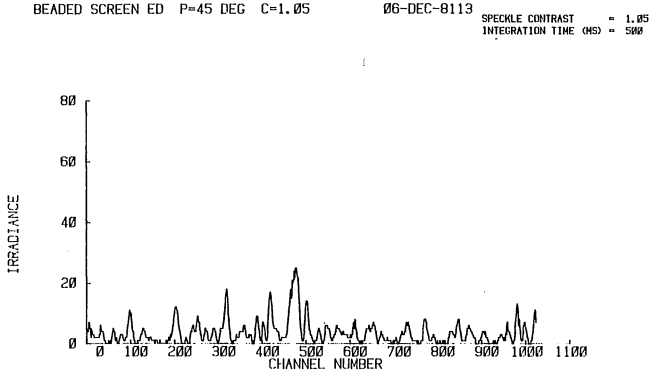

(a)

Fig. 6.3. Polarized speckle from a beaded screen.

(a) Polarization angle = 45°.

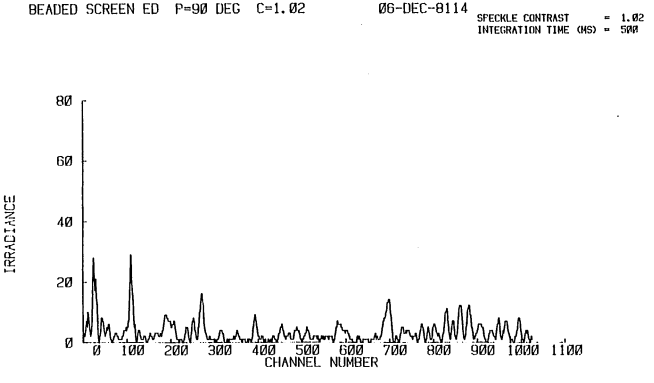

(b)

Fig. 6.3.--Continued

(b) Polarization angle = 90°.

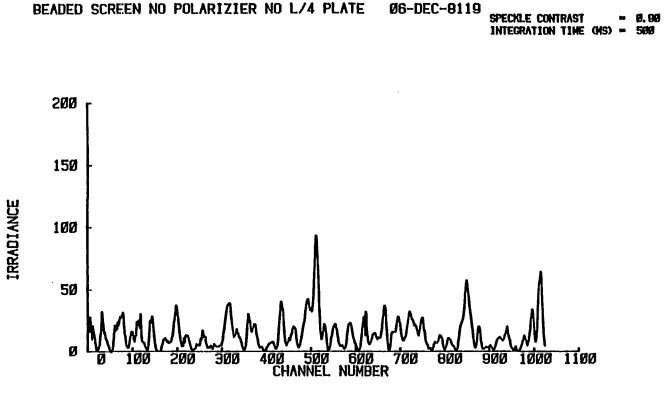

Fig. 6.4. Unpolarized speckle from a beaded screen, no quarter wave plate in the incident beam.

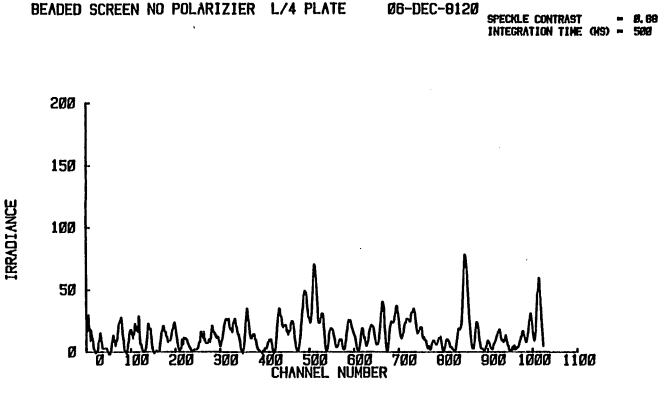

Fig. 6.5. Unpolarized speckle from a beaded screen with a quarter wave plate placed in the incident beam.

Table 6.1. Contrast from uncoated screens-unpolarized.

Ordinary Beaded (Edmund Scientific)	.86
Ground Glass Plate	.93
High Gain Beaded (3M 7610)	.83
High Gain Beaded (3M 7615)	.79
Metallic (Scotch 5430)	.90

partially correlated speckle patterns that are generated at different polarizations. It is not necessary to introduce any polarization modulation into the laser beam due to the internal depolarization by the screen itself.

Speckle Diversity by Changing the Angle of Illumination

Another technique to create a diversity of speckle patterns is by changing the angle of incidence of illumination. The speckle patterns created at differing angles of illumination will be partially correlated with one another. The degree of correlation depends on the surface structure, the total change in angle, and the size of the viewers point spread function at the screen.

The decorrelation of a speckle pattern (in a non-imaging geometry) under a change in illumination was used by Leiger, Mathieu, and Perrin (1975) to measure surface roughness. In their experiment, 2 speckle patterns are recorded on the same piece of film, each being illuminated from a different angle. Rotating the angle of illumination causes the speckle to translate by a fixed distance, and also to change its structure. Upon playback of the negative with collimated light, the translation of the speckle pattern between exposures creates sinusoidal fringes, and the decorrelation of the speckle pattern reduces the visibility of the fringes. The visibility is then related to the surface roughness.

For applications to laser displays, we are interested only in the contrast reduction due to decorrelation of the speckle patterns at

differing angles of illumination. Again, if the laser spot is larger than (or approximately equal to) the viewers object plane PSF, the same area on the screen must be illuminated from different angles for contrast reduction. A possible technique for implementing this idea in a scanned laser display is shown in Fig. 6.6. The window of an acousto-optic (AO) modulator is imaged onto the screen and the video signal is used to modulate the RF drive to the AO device. Thus as the mirror scans the laser spot across the screen, the video information moves across the modulator. The two must be synchronized so that the laser intensity at a single point on the screen is constant (within the window of the modulator), but is illuminated from a band of angles.

If we examine the rough surface approximated as a series of step functions with unit scattering area and random heights, the speckle pattern is created by the coherent superposition of light from each scattering center. Since the height of each center varies (and in the white noise approximation is random), each scattering center contributes a different phase to the phasor addition, forming the speckle pattern. If the angle of illumination is now changed by an angle θ, the optical path difference from each scattering center will be proportional to its height multiplied by $\cos\theta$. This new set of phasors creates a different speckle pattern which is only partially correlated with the original speckle pattern. As the angle becomes larger, the decorrelation between speckle patterns becomes greater. Also, as the size of the PSF on the surface increases, more scattering centers are included in the superposition and the total OPD across the PSF becomes larger, causing the

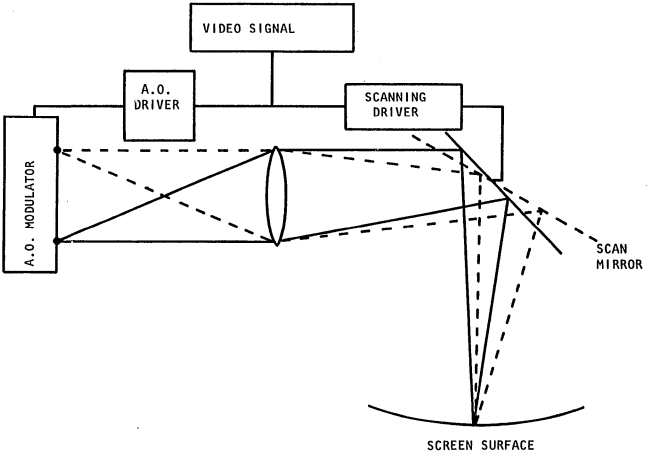

Fig. 6.6. Scan angle technique for speckle reduction in laser displays.

speckle pattern to become increasingly decorrelated. Therefore, if we incoherently sum several speckle patterns created as the angle of illumination changes, we are summing only partially correlated speckle patterns. As the scanning angle increases, or the object plane PSF increases, the amount of correlation decreases, and we expect the contrast to be reduced.

To model this process, we used a galvo driven scanning mirror to project a large (2.5 mm) collimated spot from the Argon laser onto a beaded screen (or through a ground glass plate). The scan mirror was driven at 50 hz with a triangle wave to simulate the effects of a ramp in angle space at the screen surface. The response of the mirror to the drive voltage, shown in Fig. 6.7, is to round off the edges of the triangle function. (The slew rate of the scanning system is limited by the mass of the mirror.) The effect of this small round off, if any, will be to underestimate rather than overestimate the amount of contrast reduction for a given angular scan. (The contribution from the ends of the scan will be greater than from the linear section of the scan because the speckle pattern is stationary at the turning points of the mirror. This implies that a smaller number of partially correlated speckle patterns will add over the integration period of the detector array and the contrast will be higher.) The integration time of the CCD was 500 msec, so each exposure contained 25 full scans.

The maximum angular scan, approximately 15 millirads, is limited by the size of the overlap between the laser spots at the extremes of the scan. This overlap region must be large enough to fill the CCD aperture

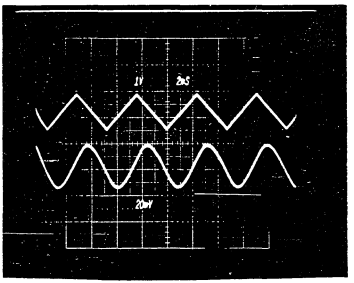

driving voltage

mirror response

Fig. 6.7. Galvonometer driven mirror driving voltage and position response of the mirror.

so that light from all angles can be integrated in the detector. The maximum scan angle is also limited by the response of the scan mirror which is a function of frequency. The minimum scan angle, about 1.2 millirads, is limited by the position feedback loop of the scan electronics which needs a minimum voltage to lock onto. The scanning angle was calibrated against the rms voltage of the position output signal from the scan electronics.

We first tested the reduction in contrast for a ground glass screen using a polarizer in front of the CCD for two values of the object plane PSF, 43 μm, and 92 μm, corresponding to F#'s of 68 and 148, respectively. We were limited in choosing aperture sizes for single CCD frames by the statistical fluctuations for F#'s much larger than 150, and by resolving the ground glass surface for F#'s much smaller than 60 (Chapter 2). Within these limitations one can see that the contrast does fall off with increasing scan angle and PSF (Fig. 6.8). The data for the 43 μm PSF (corresponding to an aperture of 5.1 mm) is presented in Appendix A. It is interesting to see how the structure of the speckle pattern changes with changing scan angle. There is some correlation between the speckle patterns at neighboring angles, but very little between speckle patterns separated by more than a few milliradians.

The contrast was also measured for the same PSF (43 μm) after removing the polarizer between the ground glass and detector. However, the difference in contrast with and without a polarizer was buried within the statistical noise of the measurement.

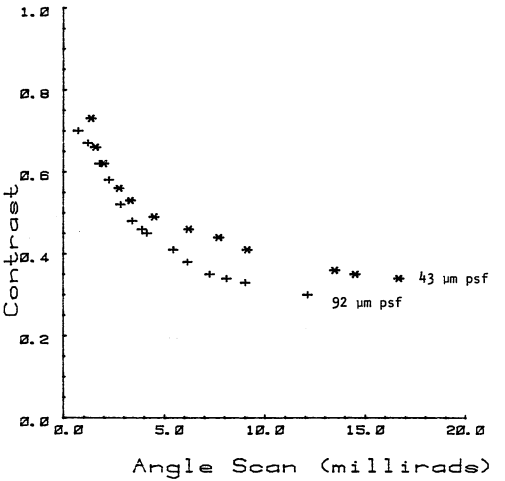

Fig. 6.8. Contrast as a function of image plane PSF for the scan angle technique.

In the second section of this chapter we noted contrast reduction due to internal polarization of light due to a beaded screen. We therefore expected some increased reduction in contrast between a beaded screen and a ground glass plate without a polarizer being present. Figure 6.9 shows the contrast measured for a beaded screen compared to a ground glass plate.

We note that when these scan angle measurements were made, we had lost the second floppy disc drive on the LSI-11. Because the software has been written to open a data file on the second disc, this did not allow us to use multiple frames for a single data set, thus limiting the accuracy of these measurements to the single frame statistical accuracy of $\approx \pm 7\%$.

This section has shown that significant speckle reduction can be achieved using the scan angle technique. The visual effect of this method is apparent from photographs of the speckle field taken with $\theta=0$ (no scan), $\theta=2.24$ millirads, and $\theta=12.40$ millirads (Fig. 6.10). While the amount of contrast reduction depends upon the viewers PSF at the screen surface, when the speckle pattern is completely resolved contrast reductions in the neighborhood of 50% to 60% should be easily obtainable (Fig. 6.9).

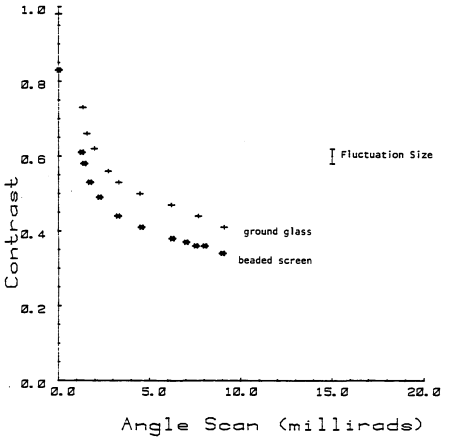

Fig. 6.9. Contrast vs scan angle from a ground glass and beaded screen.

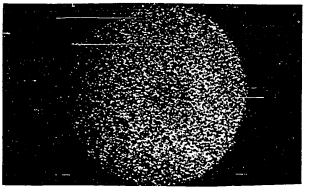

(a)

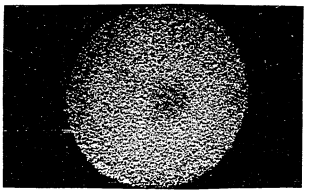

(b)

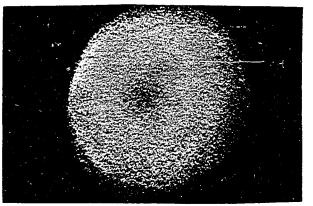

(c)

Fig. 6.10. Speckle pattern observed with the scan angle technique.

(a) No scan, θ=0.
(b) θ=2.24 millirads.
(c) θ=12.40 millirads.

CHAPTER 7

HIGH-GAIN HOLOGRAPHIC SCREENS

Along with the problem of speckle noise in laser displays is the problem of dim image formation, especially when the screen area is large. If a high-gain retroreflective screen is used, such as a high-gain beaded screen, cats eye screen, or corner-cube array, the maximum reflected radiance is always along the ray bundle from the laser projector to the screen. Thus it is impossible to place the viewer's eye in a position to intercept the maximum light without using a beam splitter or blocking the projection beam. For high brightness, the viewer must be placed close to the incident ray bundle, and the retroreflected diffraction lobe must be widened (for example, in a beaded screen by changing the size and index of the beads, Vedar and Stoudt, 1978) or in a lenticular screen by varying the index and shape of the lenticular elements (Marchand, 1975)) to include the viewer. This results in geometric constraints in the design of viewing theaters and lower-than-optimum screen brightness.

A solution to this problem is to place a hologram or diffraction grating in front of the retroreflection screen. A portion of the incident beam is split away and retroreflected at a different angle, allowing the viewer to be placed at the maximum of this split-off reflected beam. The width of the reflected diffraction lobe can then be decreased, substantially increasing the amount of light intercepted by the viewer. Figure 7.1

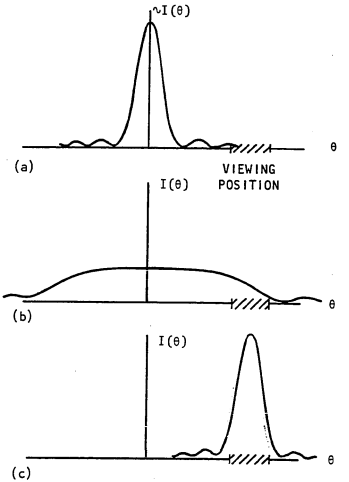

Fig. 7.1. Screen brightness as a function of viewing angle for a high-gain, beaded screen (conceptual view).

(a) Normal screen with the observer outside the high brightness viewing lobe.
(b) The high-brightness lobe widened to include the viewer.
(c) The position of the high-brightness lobe moved with a hologram to include the viewer.

illustrates the problem and the conceptual solution to the problem. A similar suggestion to increase gain for rear-projection screens by using a hologram was suggested by Meyerhofer (1973).

Theoretical Description

An example of a holographic high-gain screen is a sine-wave transmission grating placed in front of and in contact with a retro-reflecting beaded screen. This configuration wuould be useful in a flight simulator where the pilot and co-pilot are placed at an angle of $\pm\phi$ from the exit pupil of the projector.

The incident beam diffracts into a ± 1 order and an undiffracted 0 order. Each order is then reflected back to the hologram by the screen and is again diffracted into three orders. Thus there is a total of 3 x 3 or 9 orders reflected from the hologram-screen sandwich. However, several of the return orders overlap so there are only five beams leaving the screen at $\theta = 0$, $\theta = \pm\phi$, and $\theta = \pm 2\phi$, where ϕ is the diffraction angle determined by the wavelength λ and the grating spacing d.

Figure 7.2 shows an unfolded view of this process; for clarity we have separated the hologram from the screen. The first number labels the first pass (left to right) through the hologram; the second number, the return pass.

If the hologram has an efficiency of η, then the percentage P of incident light diffracted into each of the return beams from the screens is given by

$$P_{\theta=0} = 6\eta^2 - 4\eta + 1 \quad , \tag{7.1}$$

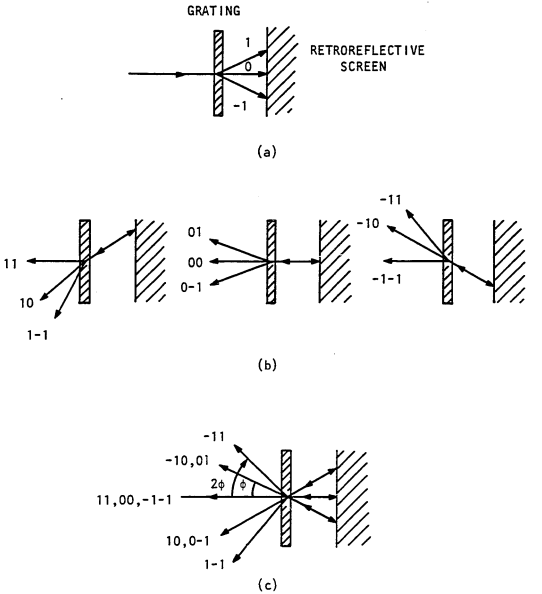

Fig. 7.2. Reflected beams produced by holographic retroreflective screen sandwich.

(a) Incident beam undergoing diffraction at the hologram.
(b) Each incident beam being retroreflected and undergoing diffraction in the return direction at the hologram.
(c) Composite of all beams.

$$P_{\theta=\pm\phi} = 2\eta(1 - 2\eta) \quad , \tag{7.2}$$

$$P_{\theta=\pm 2\phi} = \eta^2 \quad . \tag{7.3}$$

Maximizing the radiance in the $\pm\phi$ beams as a function of diffraction efficiency (Eq. 7.2) yields $\eta_{max} = 1/4$. The percentage of light in the 0, $\pm\phi$, and $\pm 2\phi$ beams becomes 37.5%, 25%, and 6.25%, respectively. The approximate increase in light over a high-gain beaded screen is given by the percentage of light in the ±1 order divided by the ratio of the solid-angle diffraction lobe of the holographic screen to the solid-angle diffraction lobe necessary to encompass pilot and copilot by an ordinary high-gain screen.

Experimental Verification

A bleached sine-wave grating of 5% efficiency was placed in contact with a 3M 7615 high-gain beaded screen. The grating was made by the interference of two collimated (plane wave) beams at angles $\pm\phi$ respectively, on a Agfa 10E56 plate which was later bleached. The retroreflected diffraction lobe from the screen is a $\text{somb}^2(d\theta/\lambda)$ function where d is the average bead size, and λ the wavelength of light, and θ is the angle between from the screen to the viewing position. When illuminated with the 488 nm line of an argon laser, the first zero of the somb function is at $\theta = \pm 0.47°$. From Eqs. (7.1) to (7.3) we expect the percentage of incident light in the 0, $\pm\phi$, and $\pm 2\phi$ beams to be 81.5%, 9%, and 0.25%, respectively. The measured percentage into the 0 and ±1 beams was found to be 64% and 7%, respectively. The radiance in the $\pm 2\phi$ beams was too small to measure. The discrepancy occurs because of losses

at the air-hologram-screen interfaces and because the screen material is not a 100% retroreflector. Losses at the interfaces could be reduced by coating the screen with photoresist and developing the hologram directly on the screen material.

Even though the hologram used had such low efficiency, the improvement in brightness over an ordinary front-projection screen was dramatic to the viewer.

Conclusions

Holographic screens may be applied to display geometries for which high brightness is required but viewing angle is limited. The general approach is to make an appropriate hologram so that when it is illuminated by the projection ray bundle, a reconstructed ray bundle generated by the hologram is reflected into the required viewing area. There is also the possiblity of using two-frequency gratings or a double-exposure hologram for projecting stereo scenes.

A drawback to these schemes is chromatic aberration in multicolor displays. In some situations this can be corrected by varying the illumination angle for differing wavelengths so that the reconstructed beams register correctly. In other systems the retroreflected diffraction lobes could be made larger than the angular spread that is due to wavelength so that the reconstructed beams would register correctly over the central portion of the viewing area.

A second drawback to holographic screens is the size of the screen that may be produced in a single exposure. For systems where the angle between the viewer and screen remains constant as different portions

of the screen are illuminated, a single hologram could be made and reproduced to form the screen. For other systems where the angle does change, the screen could be made as a mosaic of different holograms.

CHAPTER 8

CONCLUSIONS

Speckle noise is an integral part of any laser projection display because it is the nature of laser (coherent) illumination to form interference patterns. Under a contract from the Naval Training and Equipment Center (who had built a large scale monochromatic laser display), we began to investigate techniques to minimize the speckle noise inherent in laser displays. While we wished to eliminate the subjective sense of image degradation, we needed an objective way to quantify and measure speckle noise. The traditional measure of the amount of speckle present under coherent illumination (or the degree of development of a speckle pattern) in the optics literature is the ratio of the standard deviation of the irradiance to the average irradiance, called speckle contrast. It was thus natural to adopt contrast as the measure of speckle noise, and compare different techniques for speckle reduction by comparing the contrast obtained with each method. Since the speckle pattern is actually formed by the viewer's eye on the retina, an instrument was needed to measure image plane speckle contrast.

Image plane contrast has been measured previously by scanning the speckle pattern with a photomultiplier tube (PMT). The reasons for using PMTs have been the high sensitivity and large dynamic range necessary for measuring the speckle field whose most likely value is zero, but in which there are also large fluctuations. CCD detector arrays, which have only

become well developed and commercially available over the last four or five years, do not achieve the sensitivity levels of PMTs under normal operating conditions (i.e., without cooling the detectors to liquid nitrogen or lower temperatures). They do have sufficient sensitivity and dynamic range to effectively measure speckle contrast, provided that the fixed pattern noise (popcorn noise) can be subtracted from the image, and the thermal dark noise can be reduced. Since a CCD removes the necessity to mechanically scan the image (or partially removes the scanning requirement depending upon the size of the array, and the statistical accuracy of the experiment required), we built an instrument for measuring contrast by interfacing a Fairchild linear CCD to an LSI-11 microcomputer.

There are two coupled problems associated with measuring contrast using a detector array. The first is that the non-uniform spatial frequency response (MTF) of the array lowers the measured value of the contrast. The second is that the relatively small number of pixels (1024) and the large speckle size (necessary so that the MTF of the array does not substantially lower the contrast) reduces the number of speckles within each detector frame. This small sample space increases the statistical uncertainty of the measurement.

The effect of the MTF on the contrast can be calculated by finding the area underneath the measured power spectrum which, if properly normalized, is proportional to the square of the contrast. (The measured power spectrum is the power spectrum of the electrical signal from the detector array, and is the product of the square of the MTF and the power spectrum of the indicent speckle pattern on the array.) For $\lambda \lesssim 600$ nm,

the MTF is limited by the finite spacing and size of the detector pixels. In this case, lowering the contrast is due to spatial averaging of the speckle pattern by the detector pixels. For $\lambda > 600$ nm, the MTF is further degraded by photo-electron diffusion within the bulk silicon of the detector chip. The effect of charge transfer inefficiency on the contrast is negligible. While the effects of the MTF on the contrast are studied in detail in Chapter 2, we can conclude that, for $\lambda \lesssim 600$ nm, the reduction in the measured contrast will be less than 5% provided that the effective F# of the imaging lens is $\gtrsim 100$. If the F# is ≥ 180, the reduction in contrast will be less than 2%.

The second problem, the statistical uncertainty in the measurement due to the limited sample space, was avoided in most of our measurements by using data from more than a single CCD frame to calculate the contrast. A computer controlled stage moves the sample under study between measurements, and the data from 40 CCD frames is written on disc. The contrast is then computed by treating all 40 frames as a single data set. In this way we were able to reduce the uncertainty of the experiment due to statistical fluctuations below the instrumental uncertainty of about 2%.

However, the uncertainty due to the limited sample space is interesting because of applications in which only one frame of data may be available. (An example of such an application might be an industrial surface roughness measurement device where the contrast is measured from machined parts on an assembly line.) The form of the statistics for the contrast, the probability density function for contrast, was calculated for a completely developed speckle pattern using a Monte-Carlo simulation.

This simulation explained the large spread in the data we observed for contrast measurements of a fully developed speckle pattern, and also explained the shift in the average speckle contrast (for many measurements) to being slightly lower than 1.

While the MTF of the detector array is fixed, the power spectrum of the incident speckle is bandlimited with cutoff frequency $1/\lambda F\#$. The effective measurement bandwidth, and thus the effect of the CCD MTF on the speckle contrast, can be changed by changing the F# of the imaging lens. Again, the details of the simulation and a discussion of the trade-offs between fine sampling (the effect of the MTF on the contrast) and coarse sampling (many statistically independent data points) is found in Chapter 2. While a best case compromise depends upon the specific application, we show that using a 1024 element array and accepting a 3% decrease in the measured average contrast would yield a statistical confidence (the one sigma point, or about a 68% confidence level) of about 4%.

The instrumentation was based on a first generation CCD donated by the Naval Training and Equipment Center along with an electronics board that generates the correctly phased timing signals for operating the CCD. The Fairchild #131 linear CCD has 1024 13 x 13 μm pixels and two separate data ports. An interface electronics box was built that acted as the bridge between the LSI-11 and the experimental world. This box contains power supplies, master clock, circuitry to amplify and combine the two separate data channels into a single data channel, electronics to synchronize the valid video data to the A-to-D on the LSI-11

bus and to synchronize the data strobe line from the LSI-11 to the master clock, and interface circuitry for running the sample stage, laser shutter, and measuring laser power and array temperature.

The major experimental problem was the thermal noise and the fixed pattern noise generated over the extremely long integration times necessary to achieve reasonable signal-to-noise ratios. Integration times were typically from 300 to 600 ms. Three different ways of reducing the noise terms were employed. First, the operating temperature of the array was reduced 24°C by attaching a thermoelectric cooler to the backside of the array, increasing the signal-to-noise by approximately 8. Secondly, 16 exposures of each frame were averaged to increase the signal-to-noise by about 4. Finally, an equal number of dark frames were subtracted from data frames to remove the fixed pattern noise. We found that it was not necessary to correct for individual pixel responsivity, although software was incorporated in the instrument operating system for this purpose. An optical wedge was indexed matched to the CCD window to eliminate multiple reflections from the window.

Two different speckle reduction techniques were studied. The first involved painting or coating screen surfaces with a dye, phosphor, or paint to decrease the coherence length of light reflected from the screen. While it is difficult to see how this technique could be used with a multi-color (i.e., multi-laser) display without a complicated internal screen structure, this technique is effective for a single wavelength display. Simply spraying a screen with a layer of yellow fluorescent paint reduces the contrast 28%. A film imbedded with Rhodamine 6G, manufactured by the 3M Co., reduced the contrast by approximately

84%, but the accompanying reduction in image brightness was also quite severe.

An unresolved problem was how to obtain contrast reduction without reducing screen gain. The samples we used to test for contrast reduction were made by coating beaded screen samples, thus covering the beads and destroying the high gain properties. An attempt was made to first coat a flat surface and then attach beads to it. We were unable however to achieve a reasonably dense or uniform bead coating, close to that obtained by commercially available high-gain screens. There is no reason in principle however, why coating the screen material first and then attaching the beads could not be done. It is possible that speckle reduction could be thus combined with high screen gain.

A second speckle reduction technique involved creating a multiplicity of partially correlated speckle patterns that appear from the same position on the screen over the integration period of the eye. The different speckle patterns are created by changing the angle of illumination while illuminating the same scattering area on the screen. One method of implementing this scan angle technique is to image an acousto-optic modulator onto the screen. If the video signal fed to the modulator is properly synchronized with the scanning optics, a single spot on the screen will be illuminated with the correct irradiance level from different angles in a time short compared with the integration time of the eye. Using a beaded screen and a reasonable laser dither of 10 millirads (reasonable because this dither represents only about .6% of the total scan angle in a 180° display) we were able to reduce the contrast by half. The advantage of the scan angle method over techniques

that reduce the coherence length of the illumination (screen coatings) are that it can be used in multi-color displays and that it will not effect image brightness. In addition the hardware modifications should not be extensive or expensive.

APPENDIX A

CONTRAST MEASUREMENTS MADE WITH THE SCAN ANGLE TECHNIQUE USING A 5.1 MM APERTURE

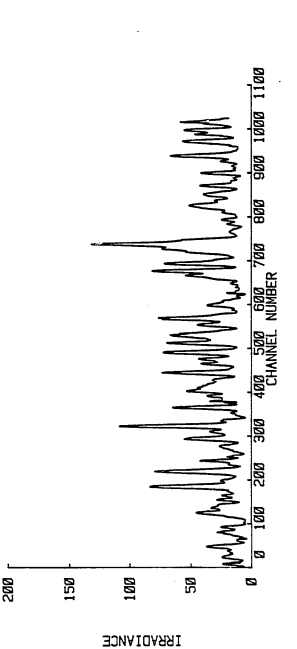
5.1 MM APERTURE THETA=1.56 C=0.66
03-DEC-8103
SPECKLE CONTRAST = 0.66
INTEGRATION TIME (MS) = 500
IRRADIANCE
200
150
100
50
0
0 100 200 300 400 500 600 700 800 900 1000 1100
CHANNEL NUMBER

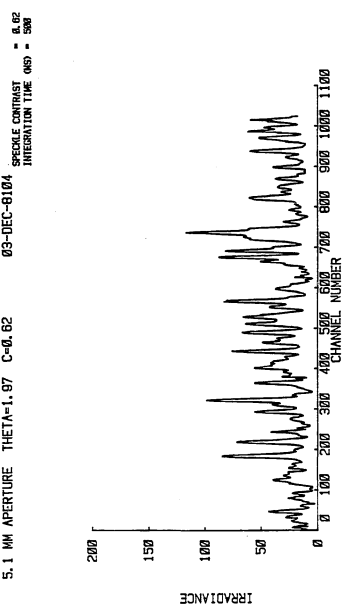
5.1 MM APERTURE THETA=1.97 C=0.62
03-DEC-0104
SPECKLE CONTRAST = 0.62
INTEGRATION TIME (MS) = 500
IRRADIANCE
200
150
100
50
0
0 100 200 300 400 500 600 700 800 900 1000 1100
CHANNEL NUMBER

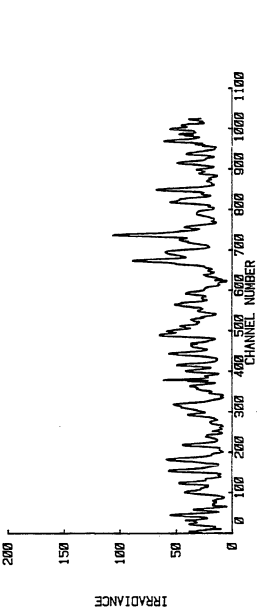
5.1 MM APERTURE THETA=4.47 C=0.50
03-DEC-0107
SPECKLE CONTRAST = 0.50
INTEGRATION TIME (MS) = 500
IRRADIANCE
200
150
100
50
0
0 100 200 300 400 500 600 700 800 900 1000 1100
CHANNEL NUMBER

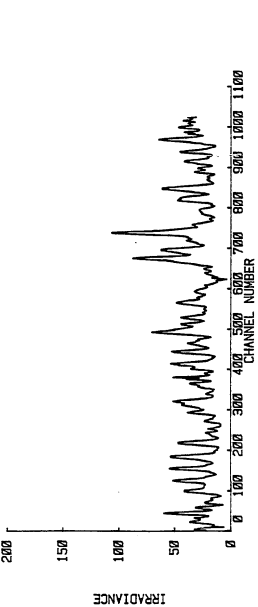
5.1 MM APERTURE THETA=6.20 C=0.47
03-DEC-0109
SPECKLE CONTRAST = 0.47
INTEGRATION TIME (MS) = 500
IRRADIANCE
200
150
100
50
0
0 100 200 300 400 500 600 700 800 900 1000 1100
CHANNEL NUMBER

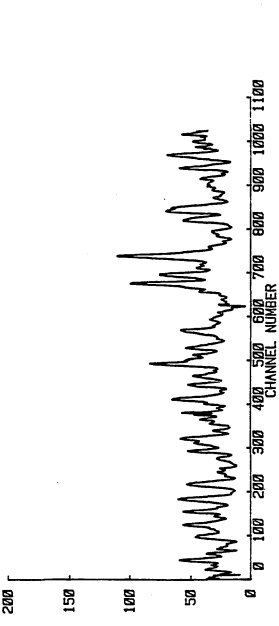
5.1 MM APERTURE THETA=7.69 C=0.44
03-DEC-0109
SPECKLE CONTRAST = 0.44
INTEGRATION TIME (MS) = 500
IRRADIANCE
200
150
100
50
0
0 100 200 300 400 500 600 700 800 900 1000 1100
CHANNEL NUMBER

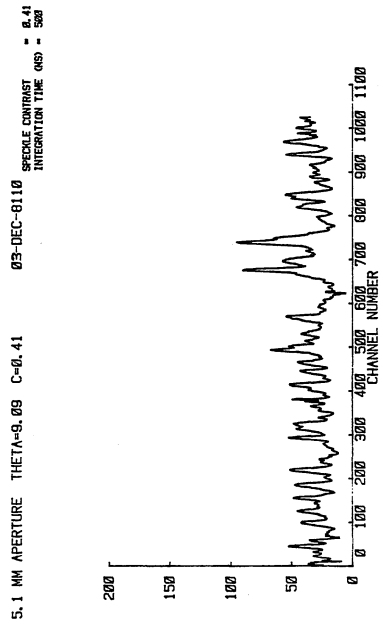
5.1 MM APERTURE THETA=9.09 C=0.41
03-DEC-0110
SPECKLE CONTRAST = 0.41
INTEGRATION TIME (MS) = 500
IRRADIANCE
200
150
100
50
0
0 100 200 300 400 500 600 700 800 900 1000 1100
CHANNEL NUMBER

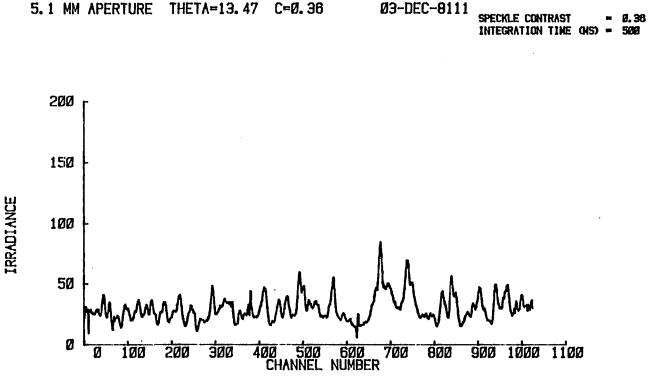
5.1 MM APERTURE THETA=13.47 C=0.36
03-DEC-8111
SPECKLE CONTRAST = 0.36
INTEGRATION TIME (MS) = 500
IRRADIANCE
200
150
100
50
0
0 100 200 300 400 500 600 700 800 900 1000 1100
CHANNEL NUMBER

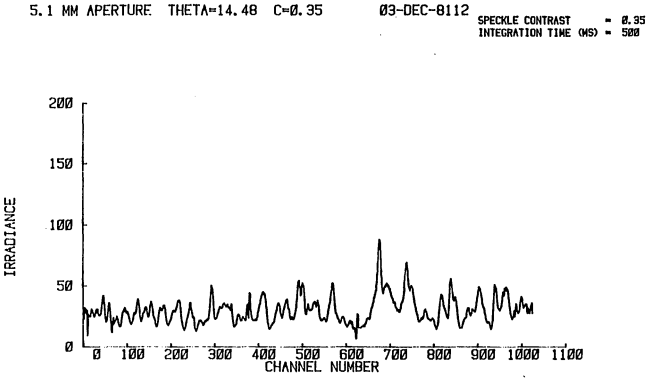
5.1 MM APERTURE THETA=14.48 C=0.35
03-DEC-8112
SPECKLE CONTRAST = 0.35
INTEGRATION TIME (MS) = 500
IRRADIANCE
200
150
100
50
0
0 100 200 300 400 500 600 700 800 900 1000 1100
CHANNEL NUMBER

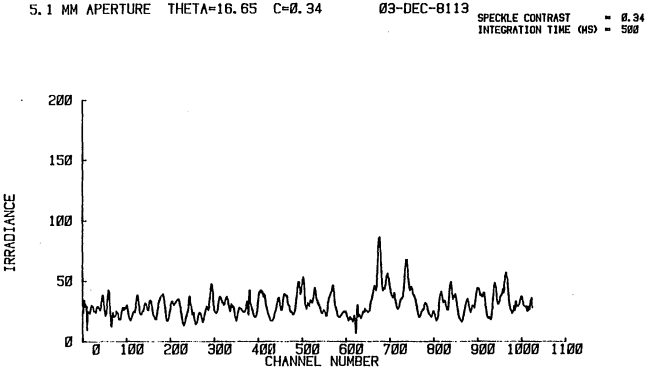
5.1 MM APERTURE THETA=16.65 C=0.34
03-DEC-8113
SPECKLE CONTRAST = 0.34
INTEGRATION TIME (MS) = 500
IRRADIANCE
200
150
100
50
0
0 100 200 300 400 500 600 700 800 900 1000 1100
CHANNEL NUMBER

REFERENCES

Asakura, Toshimitsu, "Surface Roughness Measurement," in Speckle Metrology (Robert K. Erf, ed.), Academic Press, New York, 1978.

Barakat, R., "First Order Probability Densities of Laser Speckle Observed Through Finite Size Scanning Apertures," Opt. Acta 20, 729 (1973).

Barakat, Richard and Jullian Blake, "Second-Order Statistics of Speckle Patterns Observed Through Finite Size Scanning Apertures," JOSA 68, 614 (1978).

Barbe, D. F. and S. B. Campana, "Imaging Arrays Using the Charge-Coupled Concept," in Advances in Image Pickup and Display (B. Kozan, ed.), Academic Press, New York, 1977.

Bergland, G. D. and M. T. Dolan, "FFT Algorithms," in Programs for Digital Signal Processing, Digital Signal Processing Committee of the IEEE, IEEE Press, New York, 1979.

Born, Max and Emil Wolfe, Principles of Optics, Pergamon Press, Oxford, 1975.

Cronin, D. J. and A. E. Smith, "Dynamic Coherent Optical System," Opt. Engineering 12, 50 (1973).

Dainty, J. C., "Some Statistical Properties of Random Speckle Patterns in Coherent and Partially Coherent Illumination," Opt. Acta 10, 761 (1970).

Dainty, J. C., "Detection of Images Immersed in Speckle Noise," Opt. Acta 18, 327 (1971).

Dainty, J. C. and W. T. Welford, "Reduction of Speckle in Image Plane Hologram Reconstruction by Moving Pupils," Optics Communications 3, 289 (1971).

Dyke, R., Director of Research CCD's, Fairchild CCD Corp., Mountainview, CA, private communication, 1981.

Epworth, Richard, "Modal Noise, Causes and Cures," Laser Focus, September 1981, p. 109-115.

Frieden, B. R., "Computational Methods of Probability and Statistics," in The Computer in Optical Research (B. R. Frieden, ed.), Springer-Verlag, Heidelberg, 1980.

George, Nicholas, C. R. Christensen, J. S. Bennett, and B. D. Guenther, "Speckle Noise in Displays," JOSA 66, 1282 (1976).

George, N. and A. Jain, "Speckle in Microscopy," Opt. Commun. 6, 253 (1972).

Gerritson, H. J., W. J. Hannan, and E. G. Ramberg, "Elimination of Speckle Noise in Holograms with Redundancy," Appl. Opt. 7, 2301 (1968).

Goodman, J. W., "Statistical Properties of Laser Speckle Patterns," in Laser Speckle and Related Phenomena (J. C. Dainty, ed.), Springer-Verlag, Heidelberg, 1975.

Goodman, J. W., "Some Fundamental Properties of Speckle," JOSA 66, 1145 (1976).

Leiger, D., E. Mathieu, and J. C. Perrin, "Optical Surface Roughness Determination Using Speckle Correlation Technique," Appl. Opt. 14, 873 (1975).

Leith, E. and J. Upatnieks, "Imagery with Pseudo-Randomly Diffused Coherent Illumination," Appl. Opt. 7, 2085 (1968).

Lim, Joe S. and Hamid Wawah, "Techniques for Speckle Noise Removed," Opt. Engineering 20, 472 (1981).

Lowenthal, S. and D. Joyeaux, "Speckle Removal by a Slowly Moving Diffuser Associated with a Motionless Diffuser," JOSA 61, 847 (1971).

Marchand, E. W., "Diffraction effects with lenticular projection screens," JOSA 65, 139 (1975).

McKechnie, T. S., "Speckle Reduction," in Laser Speckle and Related Phenomena (J. C. Dainty, ed.), Springer-Verlag, Heidelberg, 1975.

Meyerhoffer, D., "Holographic and Interferometric Viewing Screens," Appl. Opt. 12, 2180 (1973).

Papoulos, A., Probability, Random Variables and Stochastic Processes, McGraw-Hill, New York, 1965.

Pearson, James E., S. A. Kokorawski, and M. E. Pedinoff, "Effects of Speckle in Adaptive Optical Systems," JOSA 66, 1261 (1976).

Pederson, H. M., "The Roughness Dependence of Partially Developed Monochromatic Speckle Patterns," Opt. Commun. 12, 156 (1974).

Pinnow, D. A., L. G. Van Uitert, and M. Feldman, "Photoluminescent Conversion of Laser Light for Black and White and Multicolor Displays 2:Systems," Appl. Opt. 10, 155 (1971).

Rawson, Eric and J. Goodman, "Speckle in Optical Fibers," SPIE Vol. 243 (1980).

Rawson, Eric G., Antonio B. Nafarrate, Robert E. Norton, and Joseph W. Goodman, "Speckle-free rear projection screen using two close screens in slow relative motion," JOSA 66, 1291 (1976).

R.C.A. Commercial Engineering, RCA Electro-Optics Handbook, R.C.A. Commercial Eng., Harrison, NJ, 1974.

Scribot, A., "First Order Probability Density Functions of Speckle Measured with a Finite Aperture," Opt. Commun. 11, 238 (1974).

Siegman, A. E., An Introduction to Lasers and Masers, McGraw-Hill, New York, 1971.

Sprague, R. A., "Surface Roughness Measurement Using White Light Speckle," Appl. Opt. 11, 2811 (1972).

Van Uitert, L. G., D. A. Pinnow, and J. C. Williams, "Photoluminescent Conversion of Laser Light for Black and White and Multicolor Displays 2:Materials," Appl. Opt. 10, 150 (1971).

Vedar, K. and M. D. Stoudt, "Retroreflection from spherical glass beads in highway pavement markings," Appl. Opt. 17, 1859 (1978).